

Developing robust methods for the electrocardiogram derived respiration and for the detection and quantification of T-wave alternans

Master Thesis

presented by

B.Sc. Felix Conz



INSTITUTE OF BIOMEDICAL ENGINEERING
PROF. DR. RER. NAT. OLAF DÖSSEL
KARLSRUHE INSTITUTE OF TECHNOLOGY
2014

Supervisor: Dipl.-Ing. Gustavo Lenis

Eidesstattliche Erklärung

Hiermit erkläre ich an Eides statt, dass ich die vorliegende Arbeit selbstständig und ohne unzulässige fremde Hilfsmittel angefertigt habe. Wörtlich oder inhaltlich übernommene Stellen sind als solche kenntlich gemacht und die verwendeten Literaturquellen im Literaturverzeichnis vollständig angegeben. Die „Regeln zur Sicherung guter wissenschaftlicher Praxis im Karlsruher Institut für Technologie (KIT)“ in ihrer gultigen Form wurden beachtet.

Karlsruhe, den 20.9.2014

Contents

1	Introduction	1
1.1	Motivation and problem	1
1.2	Task and outline	2
2	Fundamentals	3
2.1	Anatomy and physiology	3
2.1.1	Heart	3
2.1.2	Excitation processes of cells	7
2.1.3	Electromechanical coupling and the role of Ca ²⁺	11
2.1.4	Excitation path in the heart	11
2.1.5	Electrocardiogram (ECG)	13
2.1.6	T-wave alternans (TWA)	17
2.1.7	ECG derived respiration (EDR)	19
2.2	Mathematical principals	23
2.2.1	Signals	23
2.2.2	Power signals	23
2.2.3	Discrete-time signals	24
2.2.4	Nyquist theorem (sampling theorem)	25
2.2.5	Statistical basics	25
2.2.6	Fourier transform	29
2.2.7	Principal component analysis (PCA)	32
2.2.8	Periodic component analysis (PiCA)	33
2.2.9	Upsampling	35
2.2.10	Median filter	36
2.2.11	Wavelet Transform	36
2.2.12	Discrete Wavelet Transform	37
2.2.13	DWT expressed as Multirate filter banks	37
3	State of the art	39
3.1	EDR	39
3.2	TWA	39

4 Methods	41
4.1 Datasets	41
4.1.1 MIT-BIH Polysomnographic Database (slpdb)	41
4.1.2 Fantasia Database (fantasia)	41
4.1.3 T-Wave Alternans Challenge Database (twadb)	41
4.2 Signal conditioning and filtering	42
4.2.1 Baseline wander removal	42
4.3 ECG derived respiration (EDR)	44
4.3.1 Single lead EDR methods	44
4.3.2 Comparison of all methods	53
4.3.3 Signal fusion	60
4.4 T wave alternans (TWA)	70
4.4.1 Spectral method	71
4.4.2 PiCA method	74
4.4.3 Performance	76
5 Conclusion and prospectives	79
5.1 EDR	79
5.2 T-wave alternans	80
A Appendix	83
References	93

1

Introduction

In this thesis, different methods for extracting a continuous respiratory signal out of an electrocardiogram signal are presented and compared. In a next step a way is proposed for combining signals generated by the methods to improve the accuracy of the resulting signal. In the second part of the thesis methods for quantifying the phenomenon of T wave alternans (TWA) are presented, followed by a discussion of the problems with the current definition of TWA and possible solutions.

1.1 Motivation and problem

The electrocardiogram (ECG) is an inherent part of today's clinical monitoring systems. Aside from invaluable information about a patient's heart activity it provides significant details about respiration, which is normally regarded as noise. This can be indeed put to good use since respiratory signals are required in several medical disciplines such as sleep, sports or stress research. Such as for the detection of apnoea, monitoring an athlete's fitness level or derive different stress levels by monitoring the respiration rate amongst other things. Typically, such signals are acquired through additional devices called spirometers. Each kind of spirometer employs a different technique to gather a respiratory signal. One such technique is to measure the air that flows through the nose or mouth with a thermistor that is placed in the breathing air stream. Thermistors are resistors that change their resistance depending on temperature. Exhaled air is warmer than inhaled air since the former is heated up while inside the body. By measuring the resistance of the thermistor, it is possible to distinguish between inhalation and exhalation. Another method involves placing a belt around the chest and/or the abdomen, equipped with sensors that monitor the belt expansion. When

the respiratory signal is generated from the very ECG it is called electrocardiogram derived respiration (EDR). EDR depends solely on the already available ECG signal. Therefore, no additional equipment is required and the technique is therefore cheap and effective. Another major benefit is the ability to generate respiratory signals for datasets where no respiration has been monitored. There exist several ways to extract the respiratory information out of an ECG but they only exploit certain characteristics at a time and not all together. This thesis addresses the possibility of improving traditionally generated EDR signals by combining them together.

T wave alternans (TWA), an alternating morphological change of the T waves, is believed to be a predictor of cardiovascular mortality and sudden cardiac death. Although the exact physiology leading to TWA is not fully understood, TWA can still be measured and quantified. In order to support further research in this topic at the Institute of Biomedical Engineering at the Karlsruhe Institute of Technology, it was necessary to implement algorithms that detect and quantify the TWA.

1.2 Task and outline

The task of this thesis is divided in two main parts. The goal of the first part is to develop a robust method to estimate a continuous respiratory signal from a single lead ECG signal. Therefore, different well known algorithms need to be implemented and benchmarked. With the results of the benchmark, the question should be cleared if it is possible to exploit the information contained in all of the separate algorithms signals and aggregate it to form an EDR signal that performs better than each of the single ones alone.

The second part of this thesis concerns TWA. Consequently, a method to detect and quantify the alternans has to be implemented. In this respect, the obvious choice is the in literature most commonly used spectral method. In addition, a more recent modification of the above algorithm, employing the latest signal processing methods is to be implemented. In the last part, the usefulness of the current way of quantifying the TWA is discussed.

2

Fundamentals

In this chapter the fundamentals for understanding this thesis both physiologically and mathematically are covered. The first section deals with the anatomy of the human heart, the electrophysiological processes and how they are monitored. Mathematical basics and methods are covered in the second section.

2.1 Anatomy and physiology

2.1.1 Heart

The task of the heart is to pump blood from the veins to the arteries of the two circulatory systems. The heart accomplishes this by rhythmic contraction and dilation. The contraction phase is called systole while the dilation phase is called diastole. The smaller circulatory system is the pulmonary circuit, that solely contains the lungs. The larger one is the systemic circuit which contains all other organs of the body like the heart itself, the brain, the kidneys, the organs in the abdomen and also the musculature, the skin and the skeleton. The two circulatory systems are connected through the heart (see fig. 2.1).

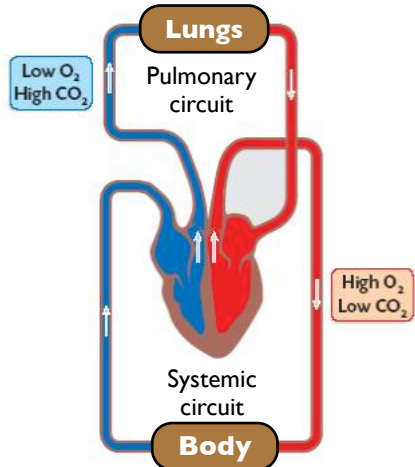


Figure 2.1. Circuits of the heart - Adapted from [1]

The heart is located in the lower anterior part of the mediastinum which is part of the thoracic cavity (see fig. 2.2). The mediastinum is confined by the pleural cavities which contain the lungs. Viewing from the top, the heart is laterally completely framed by the lungs and to the front only partly, which is important for understanding EDR (see fig. 2.3).

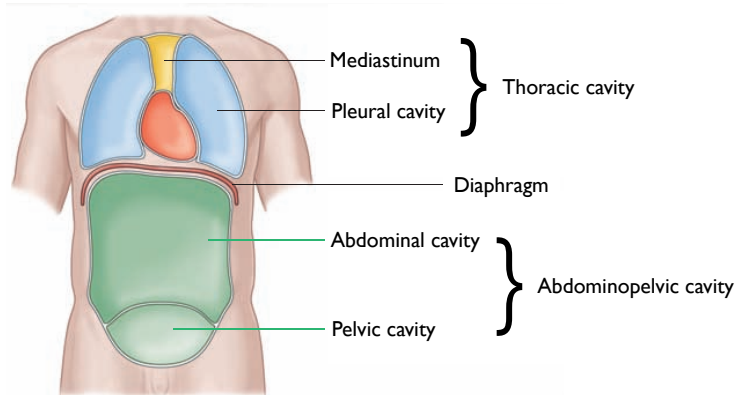


Figure 2.2. Thoracic cavities (front) - Adapted from [2]

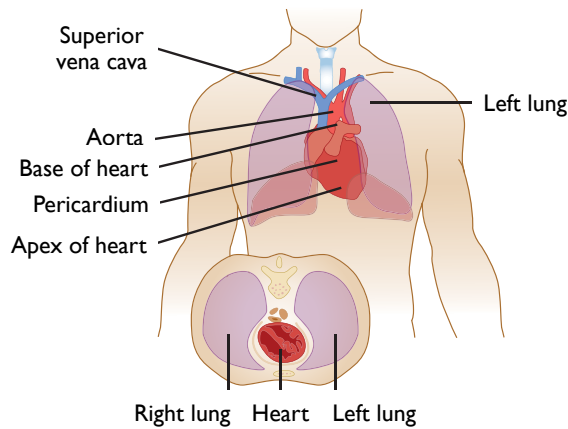


Figure 2.3. Position of heart and lungs - Adapted from [3]

The lower regions of the heart partly rests on the diaphragm, the front touches the sternum (breast bone) and the rib cartilage while the back is mostly in contact with the esophagus (the gullet). It does not directly touch its surrounding organs, instead it is fully enclosed by the heart sac (pericardium), a serous cavity which reduces friction between the heart and its neighbouring structures. Because of the spatial tightness to the breathing organs like the lungs, the diaphragm and the ribcage, the heart changes position when breathing even though it is decoupled by the pericardium.

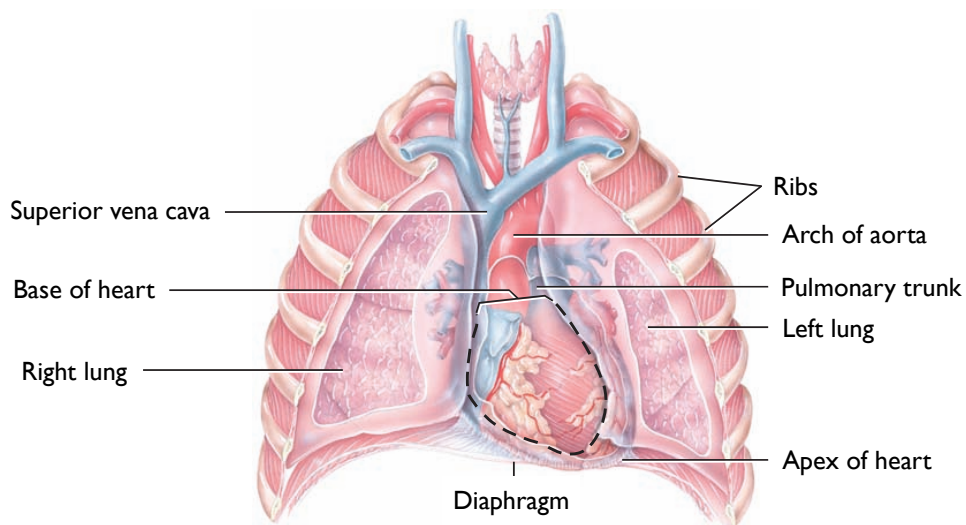


Figure 2.4. Position of heart and lungs - Adapted from [4]

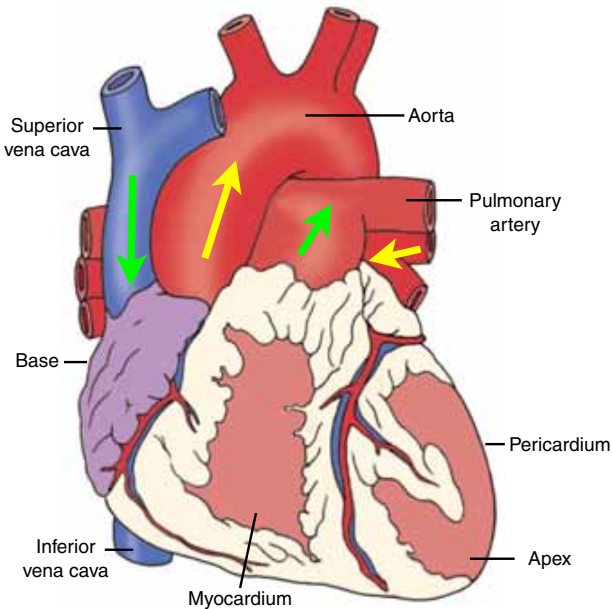


Figure 2.5. The heart (outside) with arrows indicating the blood flow from the right (green) and left (yellow) half - Adapted from [3]

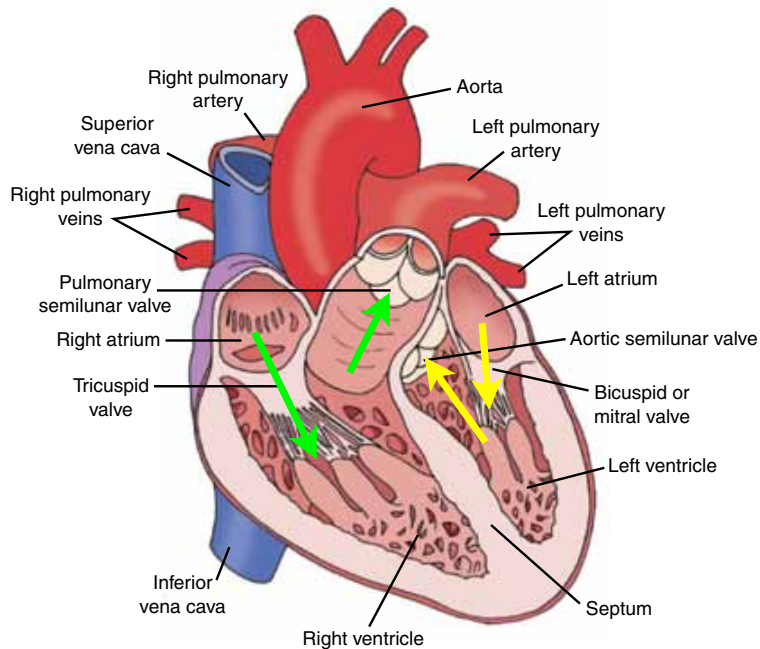


Figure 2.6. The heart (inside) with arrows indicating the blood flow from the right (green) and left (yellow) half - Adapted from [3]

The heart itself is a hollow muscular organ i.e. it consists of blood filled chambers that are enclosed by strong muscle fibres. Depending on gender, age and fitness level of a person, it weighs 250-400 g and is about the size of the persons' fist. One can divide the heart into two halves, left and right. Each half contains an atrium and a ventricle (see fig. 2.6). The pulmonary circuit is connected to the left atrium and the right ventricle, the systemic circuit is connected to the right atrium and the left ventricle (see fig. 2.1). The blood flows from the veins to the atrium that acts like a reservoir from which it then enters the ventricle. The greater pumping work is performed by the ventricle. The ventricles build up different pressures and hence their walls differ in thickness. Since the left ventricle pumps blood through the larger circuit it needs to be stronger and so the muscular walls are thicker (11 mm on the left compared to 4 mm on the right). The septum divides the right and left parts of the heart. To allow the blood flow in only one direction, there are four valves. These can be subdivided into two types, first the Atrioventricular valves which separate the atria from the ventricles and second, the Semilunar valves which are located at the connection of the ventricles to the arteries where the blood exits the heart. Section adapted from [5] and [6].

2.1.2 Excitation processes of cells

The pumping of the heart is done by the myocardium which is excited electrically. In this section, the electro-physiological basics are covered from a cellular point of view. It starts with the resting potential, which is the state of the cell when it is at rest and is followed by the explanation of an action potential that makes the myocardium contract. Both inside and outside the cell, there are ions in different concentrations. The interaction of the two enables the cell to contract.

2.1.2.1 Resting potential

At thermodynamic equilibrium the concentrations of the positive charged Na^+ and K^+ ions inside and outside the cell would be the same but there is a transportation system inside the cell membrane called the $\text{Na}^+ \text{-K}^+$ -pump that constantly pumps Na^+ out of the cell and K^+ inside. This leads to a high K^+ concentration inside the cell and a high Na^+ concentration outside. This concentration gradient leads to the diffusion of the ions. This diffusion process occurs through selective ion channels that only allow certain ions to

pass through e.g. only K^+ or Na^+ . In the resting state the cell membrane is mainly permeable to K^+ through selective K^+ channels and hence only K^+ ions diffuse. In this process the inside of the cell gets more negative and an electric field builds up between the inside and the outside which in turn leads to a second electrical diffusion process. At some point both forces that drive the diffusion are equally strong and the amount of K^+ that diffuses into and out of the cell is the same. The voltage between the outside and the inside of the cell is called the membrane potential even though it is a potential difference. This is however valid because the outside is defined as the reference point or ground. The state in which the net K^+ diffusion is zero is called the K^+ equilibrium potential (see fig. 2.7).

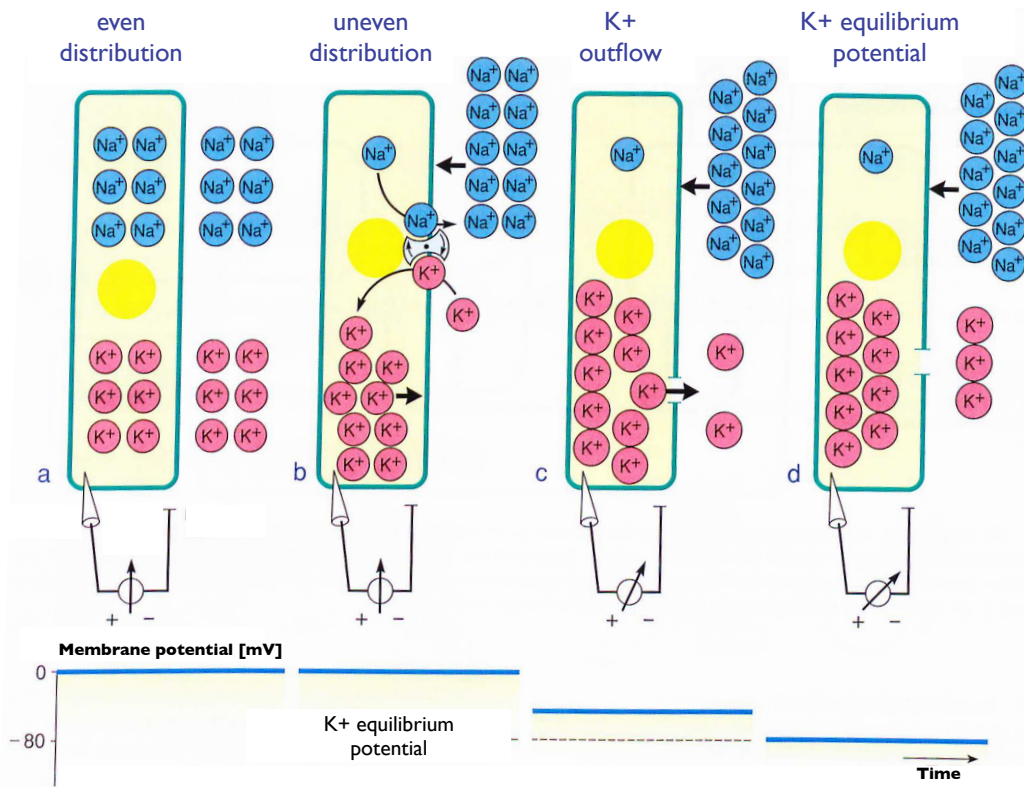


Figure 2.7. Development of the K^+ equilibrium potential - Adapted from [7]

Although there are other ions than K^+ present with similar but much less diffusion processes, the resting potential is mainly defined by the K^+ equilibrium potential. Section adapted from [7].

2.1.2.2 Action potential

The basic excitation process of a cell is a short change of the membrane potential. This process in which the inside of the cell gets positive is called action potential. Each cell contains voltage controlled selective ion channels. These channels for K^+ , Na^+ or Ca^{2+} change their permeability when the membrane potential is changed. The channels can have three different states. First they can be closed and activated by a depolarisation. Second they can be opened by depolarisation. In this state the ions can pass the channel. Third they can get deactivated or blocked during depolarisation and can only be unblocked by a repolarisation. The course of one action potential can be divided into three phases: depolarisation, “plateau phase” and repolarisation. After an action potential is triggered by the neighbouring cells causing a potential elevation of at least 15 mV, a rapid depolarization starts. The threshold at which this depolarization starts is between -70 and -75 mV for a typical resting potential of -90 mV. If this threshold is not reached no action potential is triggered. The fast depolarization (1-2 ms) causes the membrane potential to reach a value of approximately +30 mV. After this peak, a first partial depolarization follows. During that a “plateau” is formed in the voltage plot (typical for a working myocardium) before the resting potential is reached again (see fig. 2.8). The duration of an action potential depends on the heart rate and varies between 180 ms at high rates and 400 ms at low rates. It is much longer than that of other cells which have typical action potential durations around 1 ms. The initial potential jump is caused by a short opening of many Na^+ channels leading to a Na^+ flow into the cell. These channels are deactivated rapidly so the Na^+ equilibrium potential of approximately +65 mV is not reached. In the next phase an inward flow of Ca^{2+} and outward flow of K^+ , whose effects on the membrane potential are approximately the same in that phase cause the “plateau” in the potential plot. The total repolarization is caused by the decrease of Ca^{2+} flow and more importantly by the increased outward K^+ flow.

Refractory phase: During an excitation process the myocardium is in a so called refractory state wherein its ability to excite is abrogated or reduced. During the fast depolarization, the “plateau” or the successive repolarisation phase (down to about -40 mV), no action potential can be triggered irrespective of the trigger strength. This is called the absolute refractory phase. In the following relative refractory period (down to approximately -75 mV) the

excitation is gradually restored. Though an action potential can be triggered here it mandates a depolarization that is stronger than usual. This typically means a rise that is more shallow, with a lower amplitude, shorter duration and a slower transmission. When an action potential is triggered in that phase the Ca^{2+} disposal inside the cell is reduced resulting in a lower contraction amplitude of the myocardium.

The long action potential duration of several hundred ms and its linked refractory period prevent the premature re-contraction by excitations returning to already depolarized cells. This suppresses a “circulation” of an excitation which would otherwise lead to uncontrolled heart contractions. Furthermore the long refractory period allows the myocardium to relax and the chambers to be refilled with blood for the next pumping cycle. Section adapted from [5].

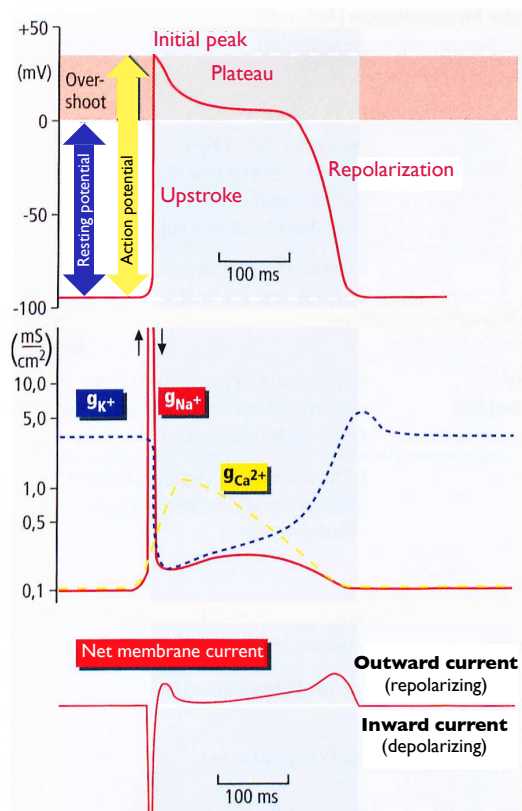


Figure 2.8. Course of an action potential (top), ion permeability (middle), net membrane current (bottom) - Adapted from [5]

2.1.3 Electromechanical coupling and the role of Ca^{2+}

The action potential reaches the inside of the cell through the plasma membrane and it is here that it triggers the release of Ca^{2+} from the Ca^{2+} -reservoirs of the cell (sarcoplasmic reticulum). This subsequently increases the Ca^{2+} concentration inside the cell. In addition to those from the reservoirs, more Ca^{2+} flows into the cell through the cell membrane due to the large concentration gradient across it. Through more complex processes the increasing Ca^{2+} concentration inside the cell activates more Ca^{2+} channels. This incoming Ca^{2+} has two effects. Firstly, it triggers the release of calcium from the sarcoplasmic reticulum and the mitochondria (Ca^{2+} induced Ca^{2+} release). Secondly, it is used to refill the reservoirs of the sarcoplasmic reticulum and the mitochondria during the diastole. This refilling process is done by ATP-powered Ca^{2+} pumps. More Ca^{2+} is transported out of the cell by a permanent $\text{Na}^+/\text{Ca}^{2+}$ exchanger. The incoming Na^+ is transported out by the Na^+/K^+ ATPases (enzymes that are constantly pumping 3 Na^+ ions out of the cell and 2 K^+ into the cell).

Electromechanical coupling describes all processes that translate electrical excitation into mechanical contraction. The exact processes how the contraction takes place and tension is build up in a muscle is described in the “actin and myosin cross-bridge cycling” process and rather complex but not relevant for this thesis. More important is the fact that the contraction is triggered by Ca^{2+} . It is the key ion for activating a mechanical contraction. An increase of the intracellular Ca^{2+} concentration activates the “actin and myosin cross-bridge cycling” leading to a contraction. This process is deactivated as soon as the intracellular Ca^{2+} concentration decreases and the muscle relaxes. Therefore the amount of Ca^{2+} inside the cell strongly correlates with the contraction. Section adapted from [7].

2.1.4 Excitation path in the heart

The regular contractions of the heart are characterized by a contraction of the atria followed by a contraction of the chambers after a short delay. To achieve this, a complex excitation conduction system is present. The contractions happen regularly and are auto generated by this system. It consists of specialized cells for excitation conduction rather than for contraction and these cells are especially developed at their interconnects.

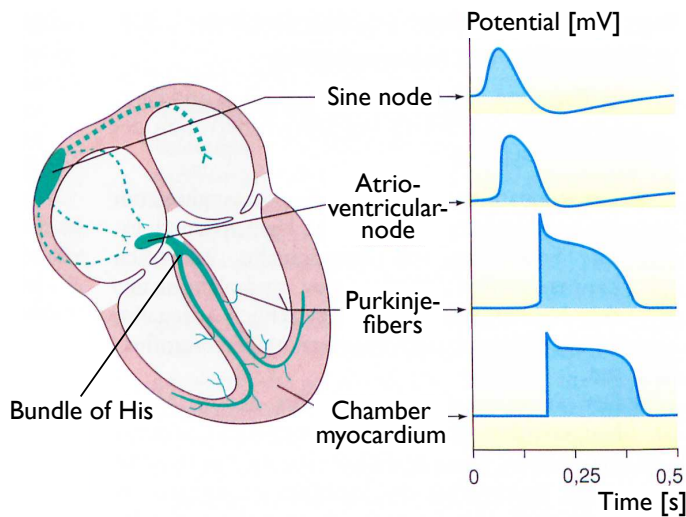


Figure 2.9. Excitation components with their action potentials over time - Adapted from [7]

Its main components are the sinoatrial node (SI node), the atrioventricular node (AV node), the bundle of His and the Purkinje fibers (see fig. 2.9). The rhythmic contractions of the heart are triggered electrically by action potentials (see section 2.1.2). The origin of these excitations is usually the sine node. The cells of the SI node are able to spontaneously generate action potentials and this lays the foundation for the automated control of the heart rhythm. It constitutes a group of cells (1-2 cm in diameter) located at the right atrium close to the junction of the vena cava. The excitation continues through internodal pathways over the working myocardium of both atria to the atrioventricular node (AV node) with a velocity of $0.6-1 \frac{m}{s}$. The conduction velocity in the AV node is only $0.05-0.1 \frac{m}{s}$, which retards the excitation. This delay enables the atria to fully contract prior to the onset ventricular contraction. From the AV node the excitation propagates through the bundle of His which is the only conducting connection between the atria and the ventricles. It splits after only a few mm into two separate branches for each of the chambers called the left and right Tawara branches. At the end of the conduction system are the Purkinje fibres that are small abducent fibres of the bundle of His. They are directly connected to the working myocardium. The excitation velocity from the bundle of His through the Purkinje fibres is high ($2-4 \frac{m}{s}$) so the ventricles are excited in a short time of approximately 70 ms.

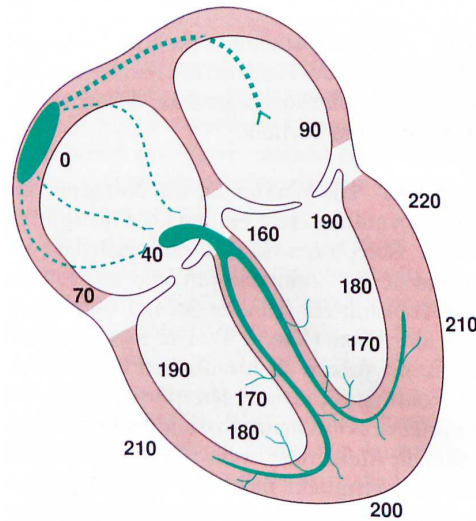


Figure 2.10. Excitation path with times in [ms] - Adapted from [7]

When an excitation is initiated at one point in the working myocardium of the atria it will continue to excite all of it (all-or-none law). The course of an excitation cycle with relative times is pictured in fig. 2.10. Section adapted from [5].

2.1.5 Electrocardiogram (ECG)

The electrocardiogram (ECG) is a method for recording and visualizing the electrical activity of the heart. Such activity generates electrical fields that permeate through the different tissues and fluids around the heart to the surface of the skin. The generation of an electric field depends on the presence of both depolarized and inactive muscular cells having different potentials. Fields in turn generate electrical potentials on the skin surface that can be measured by means of contact electrodes. The potential difference between different places on the skin is low, typically in the range of 1 mV, compared to the membrane potential in the range of 120 mV. This potential difference can be seen as a voltage between two electrodes. [7]

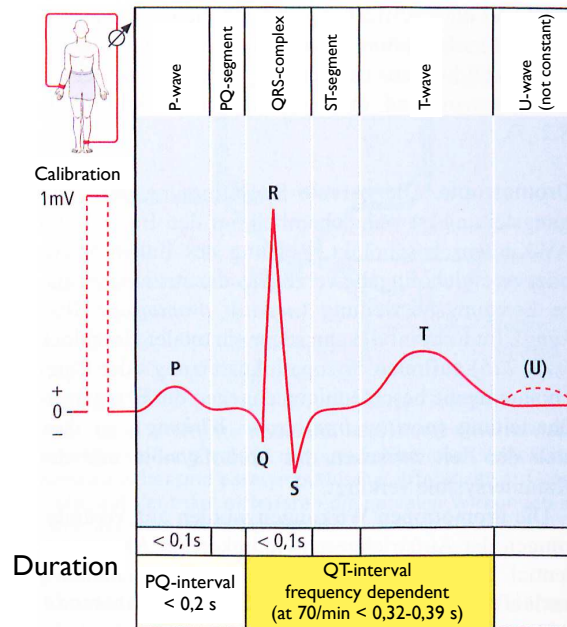


Figure 2.11. Description of waves and segments in a typical ECG trace (Einthoven II) - Adapted from [5]

The basic appearance of an ECG is substantially dependant on the excitation path inside the heart and the ECG lead configuration. The voltage changes are best visible in the leads between the right arm and left leg (Einthoven II). A typical ECG trace is displayed in fig. 2.11. There are peaks and waves visible with positive and negative deflections which are denoted with letters from P to U. The zero line is called the isoelectric line.

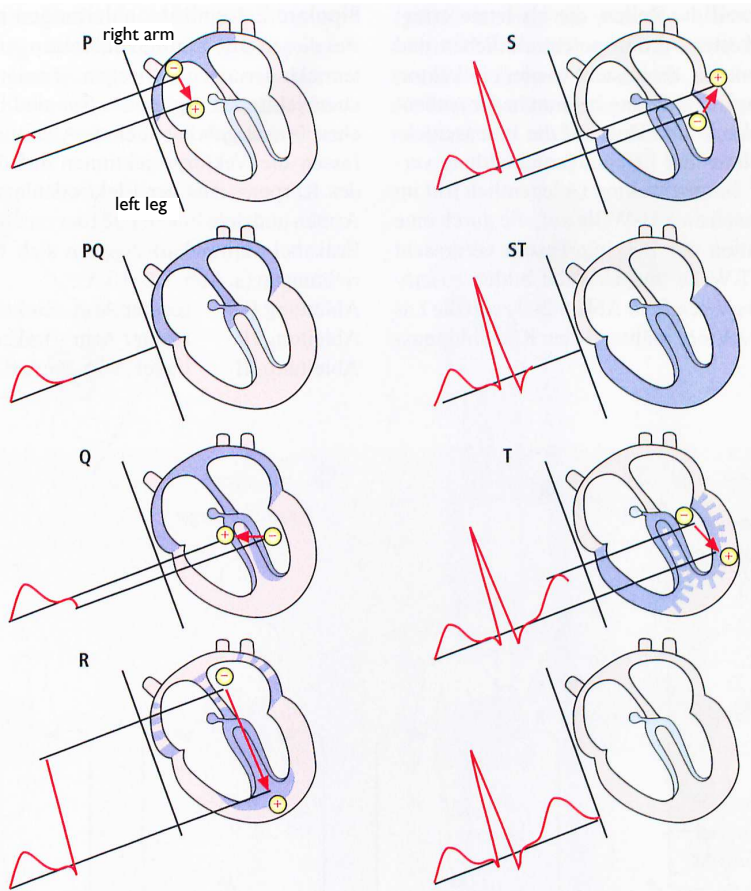


Figure 2.12. Development of an ECG trace with depolarized (blue) and repolarized (grey) regions
- Adapted from [5]

The excitation path in the heart is seen in the different waves of the ECG (see fig. 2.12). The beginning of the excitation occurs in the atria which is depicted in the ECG as the P wave. At the end of the P wave is the PQ interval where all atrial myocardium is excited with no visible potential difference. The PQ interval is the time between the excitation of the atria and the ventricles and includes the progression of the impulse through the AV node, the bundle of His and the Tawara's branches. However, this progression is not seen in the ECG because the voltages are too low, only the activity of the working myocardium is visible. The PQ interval ends with the depolarization of the ventricular myocardium which is seen in the QRS complex. The repolarization of the atrial myocardium is concealed by the QRS complex occurring simultaneously. Since the ventricles have a large muscle mass compared to the atria, the QRS complex has the largest amplitude in the ECG. When the entire ventricular myocardium is depolarized, there is no potential difference

and thus no deflection in the ECG until the repolarisation starts. This part of the ECG is called the ST segment. The subsequent T wave represents the ventricular repolarization. The typical durations of the different segments are listed in table 2.1.5. Section adapted from [5].

P-wave	80 ms
PQ-segment	120-180 ms
QRS-complex	80-120 ms
ST-segment	80-120 ms
T-wave	160 ms
RR-interval	600-1200 ms

Table 2.1. Duration of ECG segments

2.1.5.1 ECG lead configurations

There are three established lead configurations for obtaining an ECG recording and these are denoted by their inventors, Einthoven, Goldberger and Wilson. The leads of Einthoven and Goldberger are shown in fig. 2.13. Einthoven leads are labelled with Latin numbers “I”, “II” and “III”. Lead “I” measures the potential difference between the right and left arm, “II” between the right arm and the left foot and “III” between the left arm and the left foot.

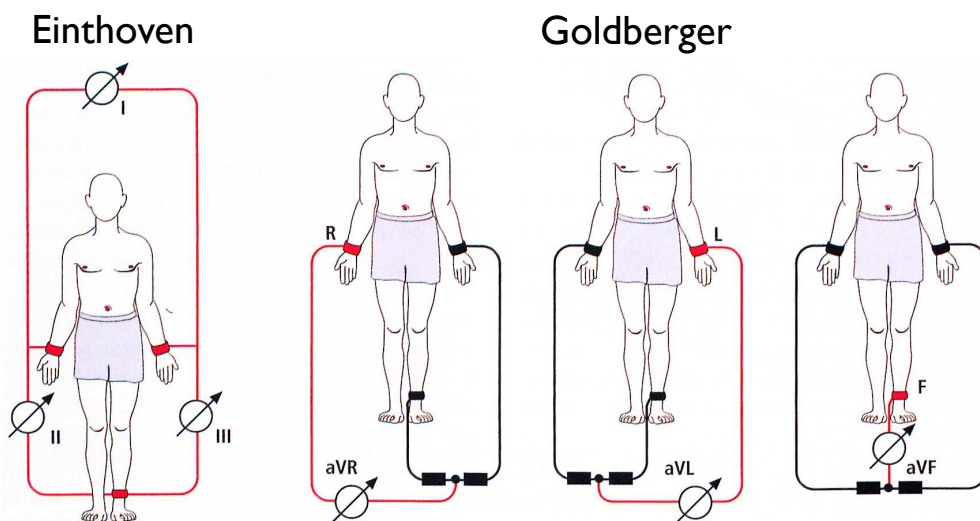


Figure 2.13. ECG lead configurations for Einthoven and Goldberger leads - Adapted from [5]

The Goldberger leads are labelled with “aVR”, “aVL” and “aVF”. Here two leads are connected together via resistors to form a reference potential to which the voltage of the third lead is measured against. The third lead configuration is the Wilson scheme (see fig. 2.14).

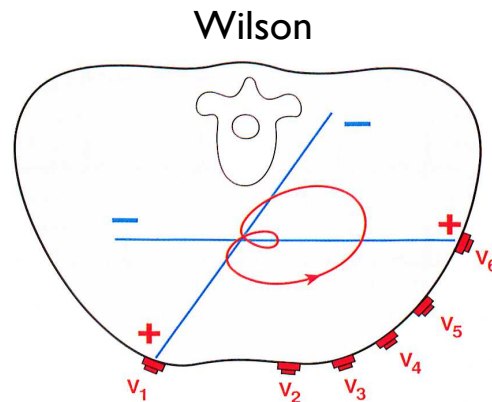


Figure 2.14. ECG lead configuration for Wilson leads - Adapted from [6]

The electrodes (V1-V6) are placed at precisely defined positions on the chest. For each position the potential of the particular lead is measured against the potential at infinity. This is approximated by connecting all three extremity leads (aVR, aVL and aVF) together through resistors to form an indifferent lead.

Each of the leads in the above mentioned configurations represents the electrical field in a specific direction in space and thus offers a spatial perspective to the electrical activity of the heart (see fig. 2.18 of section 2.1.7). Section adapted from [5].

2.1.6 T-wave alternans (TWA)

“T-wave alternans (TWA) is a beat-to-beat fluctuation in the amplitude, waveform, or duration of the ST-segment or T-wave” [8]. TWA increases with heart rate [9] that means it is only detectable when the patient is not at rest. At the moment it is unclear what exactly causes TWA however there exists a hypothesis. With reference to this, the main reason for TWA are instabilities of intracellular Ca^{2+} cycling that cause alternation in the action potential duration (APD) [10] (see fig. 2.15). Looking at the cellular level “T-wave alternans is caused by beat-to-beat changes of the membrane ionic

and intracellular processes that determine the time course of repolarization” [11] (also see section 2.1.2.2). Since TWA only occurs at higher heart rates it is most likely caused by an AP in the relative refractory period that obstructs the recovery of the cell from the previous AP. The ion current cycle of this AP is disturbed so the cell is not fully recovered (see AP2 in fig. 2.15 E). This also explains why TWA is present at lower heart rates in patients with heart diseases that influence the ion channel currents’ balance [11]. As mentioned earlier Ca^{2+} is a candidate ion for such an ion current cycle.

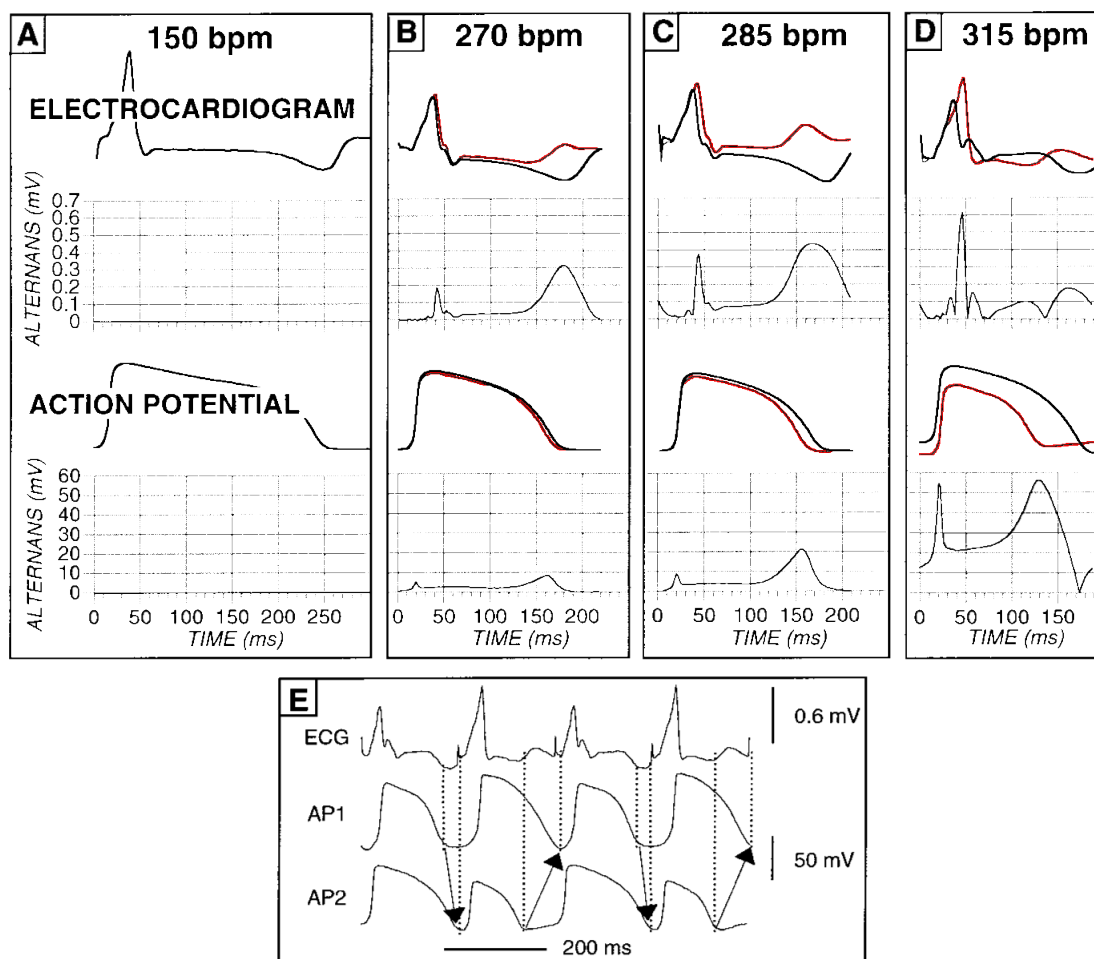


Figure 2.15. A-E: TWA in the ECG and corresponding action potentials at different heart rates (differences highlighted in red), E: ECG alongside two action potential time series at different locations - Adapted from [11]

2.1.7 ECG derived respiration (EDR)

Electrocardiogram derived respiration (EDR) is used to derive a continuous respiratory signal directly from the ECG. This provides a cheap alternative to obtaining these signals with additional devices. It is even possible to generate such a signal after the ECG has been recorded which can be interesting for established databases where no respiratory signal has been gathered simultaneously. There exist several reasons why it is possible to extract an EDR signal from an ECG signal.

The first reason is the movement of the electrodes relative to the heart. The ribcage lifts up during inspiration and down during expiration (see fig. 2.16) this means the electrodes record slightly different angles of the heart during a respiratory cycle.

The second reason is the changed permittivity of the thorax when the lungs fill with air. Since the lungs are in between the heart and the electrodes (see fig. 2.3) signal changes can be measured there. The human body contains 50–70% water [12] with a relative permittivity of $\epsilon_{r_{water}} \approx 80$ compared to the air in the lungs of $\epsilon_{r_{air}} \approx 1$. A problem with EDR is however its inability to record abdominal breathing properly because the electrodes are only placed at the upper thorax which does not move much during abdominal breathing. The third reason is the respiratory sinus arrhythmia (RSA), a variation of the heart rate with respiration. During inhalation the heart rate increases whereas during exhalation it experiences a decrease.

A major problem with this phenomenon is that some studies say it decreases with age whereas others doubt it [13]. Hence, this needs to be kept in mind when using algorithms exploiting RSA.

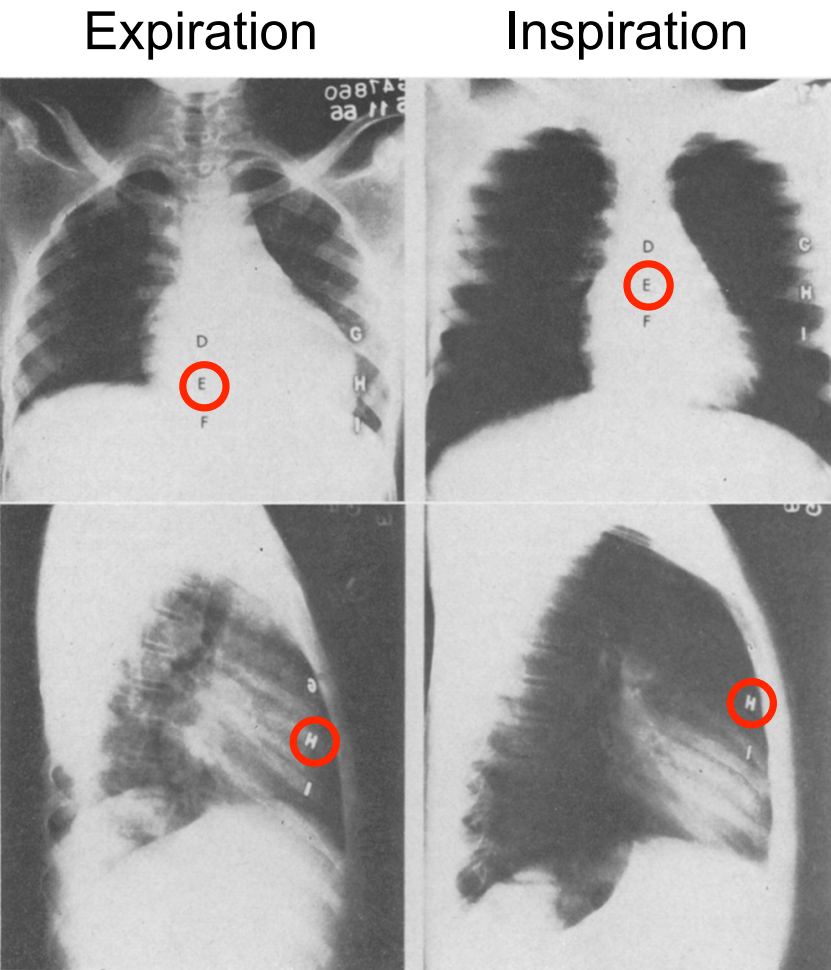


Figure 2.16. X-ray during expiration and inspiration with marked ribs - Adapted from [14]

The effects of the changing viewing angle on the heart and thorax permittivity can be interpreted as a modulation of the ECG signal. When putting this into a model, it can be expressed through equation (2.1).

$$s(t) = A \cdot n_{total,base}(t) + B \cdot s_{resp,base}(t) + ECG(t) \cdot [1 + C \cdot s_{resp,mod}(t) + D \cdot n_{total,mod}(t)] \quad (2.1)$$

The signal that is measured and available for further processing is $s(t)$, the $ECG(t)$ term is the electrical activity that is generated by the heart and all other parts are usually unwanted noise. The additive part of equation (2.1) with the coefficients A and B can be seen as the baseline while the term in squared parenthesis represents the modulating part. All noise components have a different influence which is expressed by the coefficients A to D . These

components have been summed in equation (2.2) for the parts affecting the baseline and in equation (2.3) for the parts acting as a modulation also indicated by the sub-indices.

$$n_{total_{base}}(t) = n_{cable_{base}}(t) + n_{electrodes_{base}}(t) + n_{muscular_{base}}(t) + n_{other_{base}}(t) \quad (2.2)$$

$$n_{total_{mod}}(t) = n_{cable_{mod}}(t) + n_{electrodes_{mod}}(t) + n_{muscular_{mod}}(t) + n_{other_{mod}}(t) \quad (2.3)$$

It contains all possible noise sources such as the noise from the cables originating from the ECG device and terminating at the electrodes $n_{cable}(t)$. Despite shielding these pick up electromagnetic radiation such as noise radiated by the electrical installations at 50 Hz or 60 Hz and higher frequencies due to switching loads. Additionally, the contact from the electrodes to the skin is not always perfect over time leading to the noise term $n_{electrodes}(t)$. Small tremors or movements of the muscles in the upper thorax area or the arms and legs can be seen electrically through $n_{muscular}(t)$. These are the most prominent noise sources while all others are combined in $n_{other}(t)$, for example the power line interference induced by the power supplies. Respiration can also be regarded as a noise signal that influences the ECG but is to be procured in this thesis and therefore denoted as s_{resp} . The additive part with the coefficients A and B can be interpreted as an offset or baseline wander.

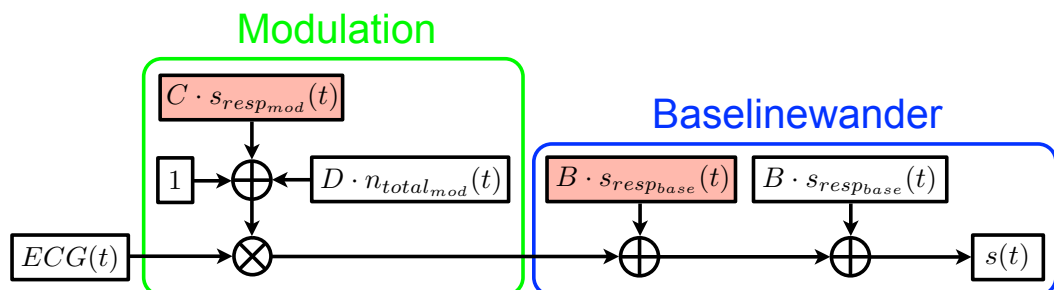


Figure 2.17. Block diagram of the signal gathered by an ECG

Since the baseline is strongly affected by other artefacts on top of respiration [15] the information needs to be gathered from the modulation. As we will later see in this thesis the influence of the unwanted noise besides the respiratory signal is much lower and hence the main cause of modulation is in fact the respiration.

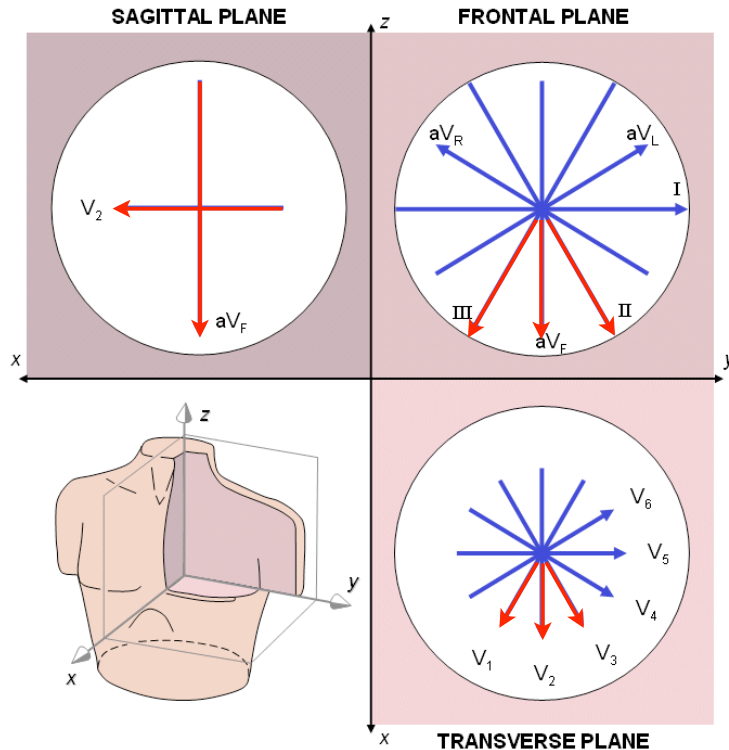


Figure 2.18. spatial direction ECG leads represent (leads mostly affected by respiration marked red) - Adapted from [16]

An important aspect is that the influence of the respiration on the morphological properties (amplitude, area, width, etc.) in the ECG is only found in certain leads. The affected leads are the ones with the strongest movement relative to the heart during breathing (see fig. 2.18). Those are in particular the leads representing the X and Z directions [17]. In X direction the leads are V₁, V₂, V₃ and in Z direction II, III and aV_F. Methods based on temporal properties (eg. RR-interval) of the ECG are not affected by this limitation.

	Min. [min ⁻¹]	Max. [min ⁻¹]	Min. [Hz]	Max. [Hz]
adults	10	18	0.17	0.3
children	20	30	0.33	0.5
infants	30	40	0.50	0.67
newborn	40	50	0.67	0.83

Table 2.2. Respiration frequencies [18]

The average respiration rate of a human is around 14 min^{-1} but varies between 10 and 50 min^{-1} or 0.17 and 0.83 Hz respectively (see table 2.2).

2.2 Mathematical principals

In this section all relevant mathematical methods are described. Vectors and matrices are illustrated in bold font such as \mathbf{x} , scalars are in italics like x . Signals with a time variable are also written in italics $x(t)$ and matrices of signals are in bold like $\mathbf{y}(t) = [x_1(t), x_2(t), \dots, x_n(t)]$.

2.2.1 Signals

A signal is a chronological sequence of an observed quantity containing for the beholder relevant information. The quantity in electrical engineering is often a voltage or current but can be any directly or indirectly measurable physical quantity. Mathematically a signal is a function from \mathbb{R} to \mathbb{R} or \mathbb{C} . There are three general signal classes energy signals, power signals and other signals. Section adapted from [19].

2.2.1.1 Energy signal

A bounded, piecewise continuous signal $y(t)$ with the converging integral

$$\int_{-\infty}^{\infty} y(t)y^*(t) dt = \int_{-\infty}^{\infty} |y(t)|^2 dt < \infty \quad (2.4)$$

is called energy signal. In this thesis all signals are of this type because of the finite number of values. Section adapted from [19].

2.2.2 Power signals

A bounded, piecewise continuous signal $y(t)$ with the diverging integral

$$\int_{-\infty}^{\infty} y(t)y^*(t) dt \quad (2.5)$$

denoting non-finite energy but an existing limit

$$\lim_{T \rightarrow \infty} \frac{1}{2T} \int_{-\infty}^{\infty} y(t)y^*(t) dt = \lim_{T \rightarrow \infty} \frac{1}{2T} \int_{-\infty}^{\infty} |y(t)|^2 dt < \infty \quad (2.6)$$

is called power signal. Section adapted from [19].

2.2.3 Discrete-time signals

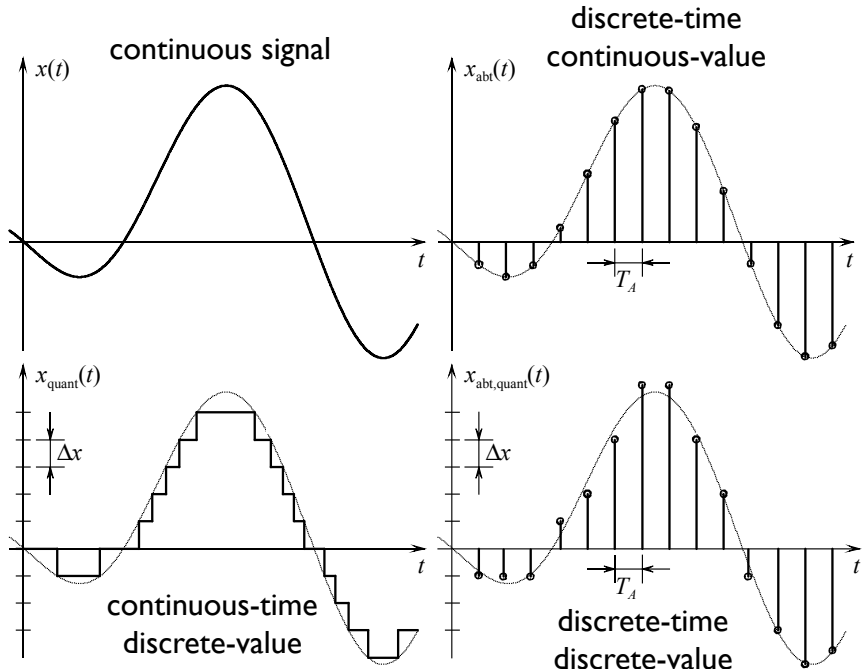


Figure 2.19. Discretization of signals - Adapted from [20]

A continuous signal has a value at any point in time. After sampling of such a signal one gets a discrete-time signal for which only values at certain equidistant points in time exist. All values in between are lost. When fulfilling the Nyquist theorem the lost values can be fully reconstructed (see section 2.2.4). A mathematical description for a discrete-time version of a continuous signal $y(t)$ is

$$y_n = y(nt_s), \quad n \in \mathbb{Z} \quad (2.7)$$

with the sampling time t_s and the corresponding sampling frequency or sampling rate

$$f_s = \frac{1}{t_s} \quad (2.8)$$

Section adapted from [19].

2.2.4 Nyquist theorem (sampling theorem)

A continuous signal $y(t)$ containing information up to a frequency f_{max} needs to be sampled with a sampling frequency f_s

$$f_s \geq \frac{1}{2f_{max}} \quad (2.9)$$

in order to retain all information. Section adapted from [19].

2.2.5 Statistical basics

This section covers the statistical basics used in this thesis. In each subsection both the general and the time discrete definitions are explained since this thesis uses time discrete signals in MATLAB®. All basics are adapted from [19] unless otherwise cited.

2.2.5.1 Random variable

Results of a random experiment is usually expressed in words such as "heads or tails" when flipping coins. For numeric evaluation these words have to be expressed in numbers. A random variable assigns each event a number such as heads gets 0 and tails gets 1. So this random variable defines a mapping of the two events to two real numbers. This can be expressed as

$$Y : \{\text{heads}, \text{tails}\} \rightarrow \{0, 1\} \quad (2.10)$$

In general it can be expressed as a mapping of the result $\omega \in \Omega$ of an event to the space of the real numbers.

$$Y : \Omega \rightarrow \mathbb{R} \quad (2.11)$$

with

$$Y(\omega) = y \quad (2.12)$$

2.2.5.2 Stochastic process

A stochastic process

$$Y : T \times \Omega \rightarrow \mathbb{R} \quad (2.13)$$

with

$$Y(t, \omega) = y \quad (2.14)$$

is a family of random variables indexed by $t \in T$. T can be interpreted as discrete or continuous time. So for a fixed $t_0 \in T$, $Y(t_0, \omega)$ is a random variable as defined in section 2.2.5.1. Whereas a fixed ω_0 leads to a time function $Y(t, \omega_0)$. This time function is called a sample function of the stochastic process.

2.2.5.3 Time discrete stochastic process

General statistics assumes an unlimited number of test functions or samples which are never available. In the discrete case one generally has only a limited number of samples per sample function and also a limited number of sample functions from which the statistics of the process $\{Y(t)\}$ have to be estimated. This kind of process is called a time discrete stochastic process with a discrete random variable.

2.2.5.4 Cumulative distribution function and probability density

The cumulative distribution function of a process $\{Y(t)\}$ represents the probability that a random function value $Y(t)$ at time t is less than or equal to y .

$$F_Y(y, t) = P\{Y(t) \leq y\} \quad (2.15)$$

The probability density of this process is then defined as

$$f_Y(y, t) = \frac{\delta F_Y(y, t)}{\delta y} \quad (2.16)$$

with the additional constraint

$$\int_{-\infty}^{\infty} f_Y(y, t) dy = 1 \quad (2.17)$$

In the discrete case with a finite number of values $x_i, i \in I, I \subseteq \mathbb{Z}$ the probability in equation (2.15) is given by

$$P(X \leq x) = \sum_{x_i \leq x} p(x_i) \quad (2.18)$$

and the probability density is

$$(p(x_i))_{i \in I} \quad (2.19)$$

with the constraint

$$\sum_{i \in I} p(x_i) = 1 \quad (2.20)$$

2.2.5.5 Moments

A stochastic process is often described by its moments. For an one dimensional stochastic process $\{Y(t)\}$ the n -th moment $\mu^n(t)$ is defined as follows:

$$E\{Y^n(t)\} = \int_{-\infty}^{\infty} y^n f_Y(y, t) dt = \mu^n(t) \quad (2.21)$$

In addition to that one can define a central moment by subtracting the first moment, the mean.

$$E\{(Y(t) - E\{Y(t)\})^n\} = \int_{-\infty}^{\infty} (y - E\{Y(t)\})^n f_Y(y, t) dt \quad (2.22)$$

For mean free stochastic processes ($E\{Y(t)\} = 0$) the n -th moment equals the n -th central moment.

In the discrete case, the n -th moment in equation (2.22) becomes

$$E\{X^n\} = \sum_{i \in I} x_i^n p(x_i) \quad (2.23)$$

and the n -th central moment in equation (2.22) becomes

$$E\{(X - E\{X\})^n\} = \sum_{i \in I} (x_i - E\{X\})^n p(x_i) \quad (2.24)$$

2.2.5.6 Mean

The mean $\mu_Y(t)$ is the first moment of a stochastic process:

$$E\{Y(t)\} = \int_{-\infty}^{\infty} y f_Y(y, t) dt = \mu_Y(t) \quad (2.25)$$

For the discrete case, equation (2.25) becomes

$$E\{X\} = \sum_{i \in I} x_i p(x_i) = \mu_X \quad (2.26)$$

2.2.5.7 Median

The median of a number of samples N is defined as follows: All samples are sorted by their value. For an odd N , the median is the value at the middle position. For an even N , the median is the arithmetic mean of the two middle values.

$$\tilde{x} = \begin{cases} x_{\frac{N+1}{2}} & , N \text{ odd} \\ \frac{1}{2}(x_{\frac{N}{2}} + x_{\frac{N}{2}+1}) & , N \text{ even} \end{cases} \quad (2.27)$$

2.2.5.8 Variance

The variance $\sigma^2(t)$ is the second central moment of a stochastic process:

$$E\{(Y(t) - \mu_Y(t))^2\} = \int_{-\infty}^{\infty} (y - \mu(t))^2 f_Y(y, t) dt = \sigma^2(t) \quad (2.28)$$

For the discrete case, equation (2.28) becomes

$$E\{(X - \mu_X)^2\} = \sum_{i \in I} (x_i - \mu_X)^2 p(x_i) = \sigma^2 \quad (2.29)$$

2.2.5.9 Standard deviation (STD)

The standard deviation $\sigma(t)$ is the square root of the Variance.

$$\sigma(t) = \sqrt{\sigma^2(t)} \quad (2.30)$$

2.2.5.10 Kurtosis

The Kurtosis is used to measure how outlier-prone a distribution is. A normal distribution has a kurtosis value of 3. The more outlier-prone a distribution is, the larger the kurtosis becomes. It is defined as the fourth central moment normalized by the standard deviation to the fourth or by the squared variance.

$$Kur\{Y(t)\} = \frac{E\{(Y(t) - \mu_Y(t))^4\}}{\sigma^4(t)} \quad (2.31)$$

For discrete processes this can be written as

$$Kur\{X\} = \frac{E\{(X - \mu_X)^4\}}{\sigma^4} \quad (2.32)$$

2.2.5.11 Cross-correlation function

The cross-correlation function is a measurement of similarity between two signals $x(t)$ and $y(t)$. For continuous signals it is defined as [21]

$$R_{xy}(\tau) = \lim_{T \rightarrow \infty} \frac{1}{2T} \int_{-T}^{+T} x(t)y(t - \tau)dt \quad (2.33)$$

For discrete signals with $m \geq 0$ it becomes [22]

$$r_{xy}(m) = E\{X^*(n) \cdot Y(n + m)\} = \frac{1}{N} = \sum_{n=0}^{N-1} x(n)y^*(n - m) \quad (2.34)$$

Negative delineations $m < 0$ can be calculated by

$$r_{xy}(-m) = r_{yx}^*(m) \quad (2.35)$$

2.2.5.12 Cross-covariance function

The cross-covariance function differs from the cross-correlation only by the product of their means [22].

$$c_{xy}(m) = r_{xy}(m) - \mu_x^* \cdot \mu_y \quad (2.36)$$

So for mean free signals ($\mu_x = \mu_y = 0$) the cross-covariance and cross-correlation functions are the same.

2.2.6 Fourier transform

The theory behind the Fourier Transform is that every continuous signal can be described by the sum of sine and cosine functions of different frequencies. For a continuous signal $y(t)$ it is defined as

$$Y(f) = \langle y(t), e^{j2\pi ft} \rangle_t = \int_{-\infty}^{\infty} y(t)e^{-j2\pi ft} dt \quad (2.37)$$

and the inverse transform is

$$y(t) = \langle Y(f), e^{-j2\pi f t} \rangle_f = \int_{-\infty}^{\infty} Y(f) e^{j2\pi f t} df \quad (2.38)$$

where $\langle \bullet \rangle$ is the scalar product of two signals. For discrete signals y_n with a limited number of values N , the Discrete Fourier Transform (DFT) is defined as

$$Y_k = \sum_{n=0}^{N-1} y_n e^{-j2\pi k n / N} \quad (2.39)$$

and often denoted as $\text{DFT}\{y_n\} = Y_k$ where its inverse operation is

$$y_n = \frac{1}{N} \sum_{k=0}^{N-1} Y_k e^{-j2\pi k n / N} \quad (2.40)$$

which is the Inverse Discrete Fourier Transform and often denoted as $\text{IDFT}\{Y_k\}$ or $\text{DFT}^{-1}\{Y_k\}$. Since it is a discrete transformation, there is a certain resolution that can be determined knowing number of samples N .

$$\Delta f = \frac{f_s}{N} \quad (2.41)$$

where Δf is the frequency resolution and f_s the sampling frequency [19]. If a signal is not stationary the DFT is applied to windows of the original signal. This is called the Short Time Fourier Transform (STFT). The window size or number of samples used for each step has to be determined depending on the application because there is always a trade-off between frequency resolution and time localization. From equation (2.41) it is clear that for higher resolution a larger number of values is needed which in turn means a worse time resolution since more samples are examined. The STFT is a function of frequency and time

$$\text{STFT}\{y(t)\} = Y(t, f) = \int_{-\infty}^{\infty} y(\tau) \cdot w(\tau - t) e^{-j2\pi f \tau} d\tau \quad (2.42)$$

where $w(\tau - t)$ is the sliding window function.

2.2.6.1 Spectrogram

The spectrogram is a graphical representation of the STFT. The absolute values of the complex FFT values $Y(t, f)$ (see equation (2.43)) are represented by a time vs frequency plot while the third dimension which is the intensity is shown by a color scale.

$$|Y(t, f)|^2 \quad (2.43)$$

The windows used for analyzing the signal usually overlap. A sample of a chirp signal with a rising frequency slope of 150 Hz s^{-1} is shown in fig. 2.20. It is sampled at a frequency of 1 kHz and analysed using a 256 points FFT with successive windows overlapping in 250 points.

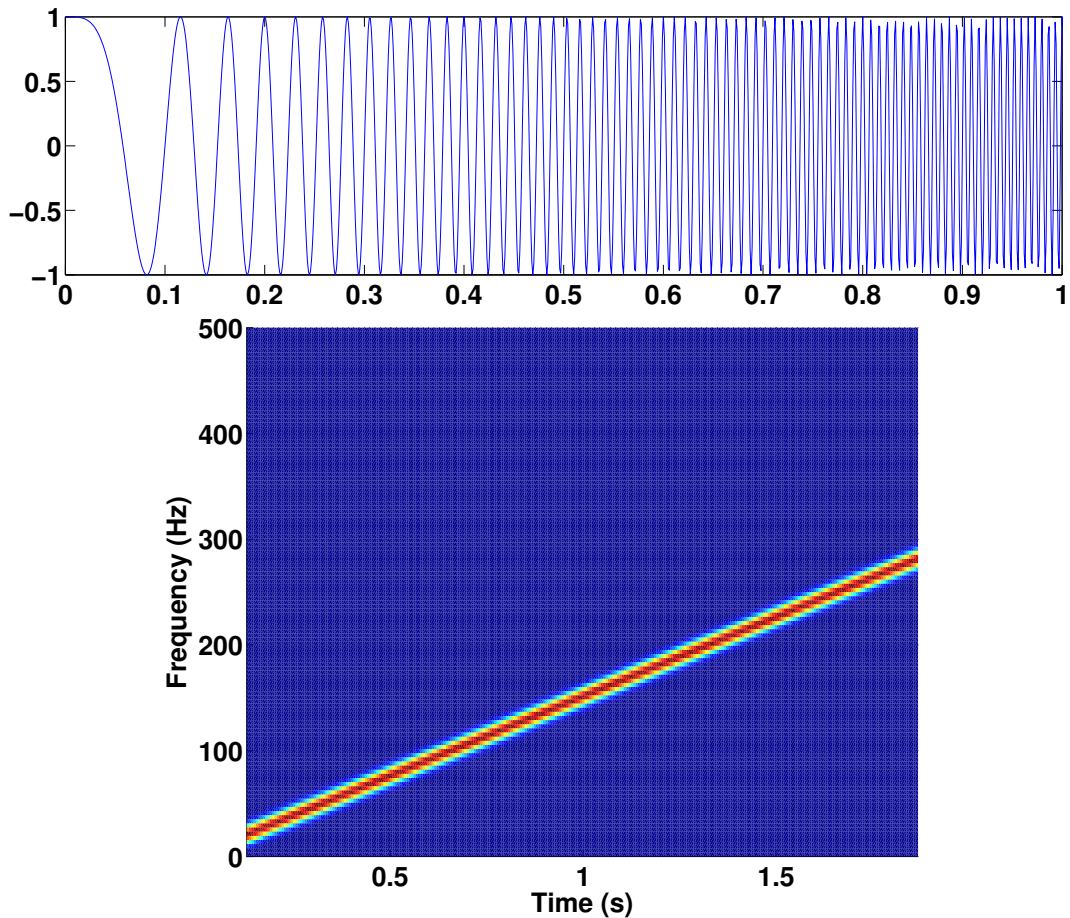


Figure 2.20. Excerpt of a sample chirp signal (top), corresponding spectrogram (bottom)

2.2.7 Principal component analysis (PCA)

Principal Component Analysis (PCA) - also referred to as time discrete Kachunen-Loève-Transformation in the signal processing field - is a signal dependant transformation that is applied to a signal that can be modelled as a realisation of a stochastic process. The goal is to create an optimal orthonormal basis of principal components in such a way that the projection of the data onto the first principal component has the largest possible variance. Each other component is chosen to be orthogonal to the previous one and maximize the variance of the corresponding projection. The variance is calculated from the observations of the underlying data set. So the principal components follow an order according to the variance they represent of the underlying dataset. It is typically used to reduce the amount of data by describing observations of a random variable only by the coefficients of the largest principal components.

PCA is an orthogonal linear transformation so it basically rotates the coordinate system in a way, that the first vector of the new basis points to the direction of the largest variance of the underlying data.

Given an ensemble of n observations of a random variable displayed as a vector

$$\mathbf{x} = [x_1, \dots, x_n]^T \quad (2.44)$$

that can be described by an orthonormal basis

$$\Phi = [\varphi_1, \varphi_2, \dots, \varphi_n] \quad (2.45)$$

through the transformation

$$\mathbf{x} = \Phi \cdot \mathbf{b} \quad (2.46)$$

the coefficients b_i can be calculated by the scalar product [23]

$$b_i = \langle \mathbf{x}, \varphi_i \rangle = \mathbf{x}^T \varphi_i^* = \varphi_i^H \mathbf{x} \quad (2.47)$$

Usually the mean values are subtracted from the original values of the observations. In the absence of this, the first eigenvector points in the direction of the mean observation so the coefficient is a measurement of its deviation from the mean value (see fig. 2.21).

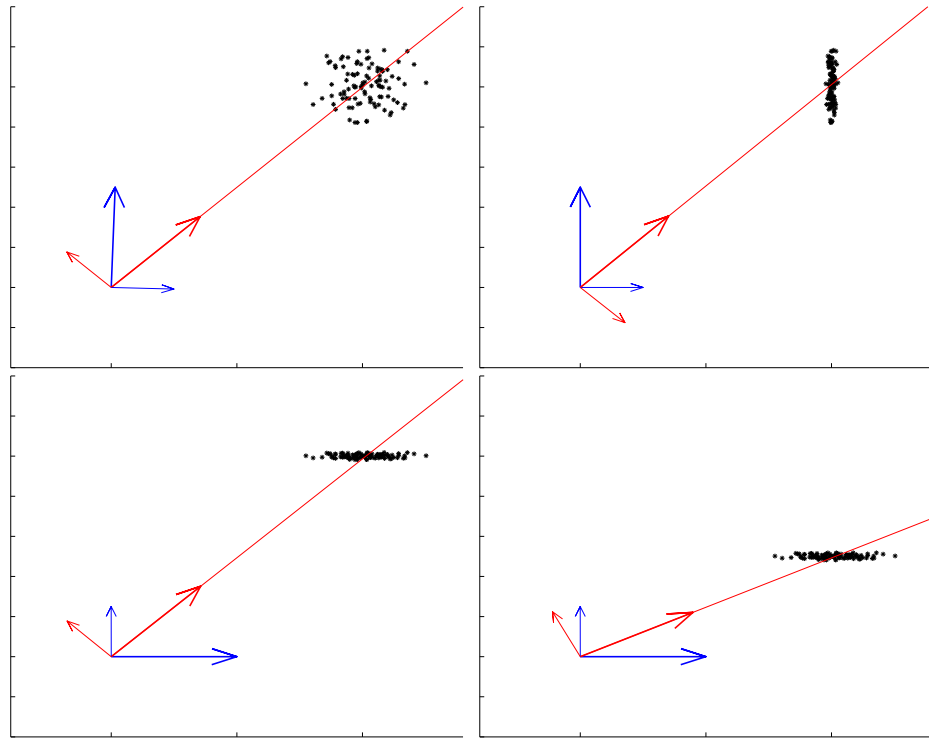


Figure 2.21. 100 observations of a 2-dimensional random value (black), corresponding principal components (arrows - bold and long: 1st PC; fine and short: 2nd PC) of centered (blue) and non-centered (red) PCA

2.2.8 Periodic component analysis (PiCA)

Periodic Component Analysis also referred to as PiCA or π CA is a linear transformation that serves to create a periodic signal with a maximized periodicity to a known period τ . This is achieved by a linear combination of those input signals $x_1(t), \dots, x_n(t)$ merged to the input signals' matrix

$$\mathbf{x}(t) = [x_1(t), \dots, x_n(t)]^T \quad (2.48)$$

and with the weighting vector $\mathbf{w} = [w_1, \dots, w_n]^T$ in such a way that the output signal

$$s(t) = \mathbf{w}^T \mathbf{x}(t) \quad (2.49)$$

is the signal with the maximized periodicity for τ . The weighting vector \mathbf{w} is found by minimizing the following quality criterion

$$\epsilon(\mathbf{w}, m) = \frac{\sum_t |s(t + \tau) - s(t)|^2}{\sum_t |s(t)|^2} \quad (2.50)$$

which is actually a measure of non-periodicity because the more periodic the signal is, the smaller the numerator becomes. In [24] it is shown that this equation can be written as

$$\epsilon(\mathbf{w}, m) = \frac{\mathbf{w}^T \mathbf{A}_x(\tau) \mathbf{w}}{\mathbf{w}^T \mathbf{C}_x(0) \mathbf{w}} = 2 \left[1 - \frac{\mathbf{w}^T \mathbf{C}_x(\tau) \mathbf{w}}{\mathbf{w}^T \mathbf{C}_x(0) \mathbf{w}} \right] \quad (2.51)$$

with the covariance matrix

$$\mathbf{C}_x(\tau) = E_t\{x(t + \tau)x(t)^T\} \quad (2.52)$$

and

$$\begin{aligned} \mathbf{A}_x(\tau) &= E_t\{[\mathbf{x}(t + \tau) - \mathbf{x}(t)][\mathbf{x}(t + \tau) - \mathbf{x}(t)]^T\} \\ &= 2\mathbf{C}_x(0) - 2\mathbf{C}_x(\tau) \end{aligned} \quad (2.53)$$

This can be solved as a generalized eigenvalue problem

$$\mathbf{C}_x(0)\mathbf{w} = \lambda \mathbf{C}_x(\tau)\mathbf{w} \quad (2.54)$$

with the candidates for lambda fulfilling

$$\det(\mathbf{C}_x(0) - \lambda \mathbf{C}_x(\tau)) = 0 \quad (2.55)$$

so equation (2.51) can be rewritten as

$$\epsilon(\mathbf{w}, m) = \frac{\mathbf{w}^T \mathbf{A}_x(\tau) \mathbf{w}}{\mathbf{w}^T \mathbf{C}_x(0) \mathbf{w}} = 2 \left[1 - \frac{\mathbf{w}^T \mathbf{C}_x(\tau) \mathbf{w}}{\mathbf{w}^T \lambda \mathbf{C}_x(\tau) \mathbf{w}} \right] = 2 \left[1 - \frac{1}{\lambda} \right] \quad (2.56)$$

by inserting equation (2.54) into equation (2.51). So the largest eigenvalue minimizes the quality criterion. The transformation matrix Ψ is now the matrix of all eigenvectors as columns of corresponding eigenvalues sorted in descending order. The transformation can be written as

$$\mathbf{y}(t) = \Psi \mathbf{x}(t) \quad (2.57)$$

With the transformed signals $\mathbf{y}(t) = [y_1(t), \dots, y_n(t)]^T$ where $y_1(t) = s(t)$ of equation (2.49). Section adapted from [24] and [25].

2.2.9 Upsampling

The method of upsampling is traditionally used as a way to increase the sampling frequency of a discrete time signal without changing the information. It can also be used as an interpolation method. The goal is to increase the sampling frequency f_A of a discrete time signal z_m by a factor L . This is done by increasing the length of the signal by L and adding $L - 1$ zeros between each sample value. This does not change the information in the signal as no energy is added. In the Frequency domain this is a periodic repetition of the spectrum. The resulting impulse series z'_n is then filtered with an ideal low-pass filter with a cut-off frequency of $\frac{f_A}{2}$ which is the Nyquist frequency of the original signal to remove the repeated spectral parts. This signal is finally amplified by L to get the upsampled signal x'_n . The resulting sampling frequency is now $f'_A = L \cdot f_A$ [23].

$$f_{nyquist} = \frac{f_A}{2} \quad (2.58)$$

The steps are visually represented in fig. 2.22.

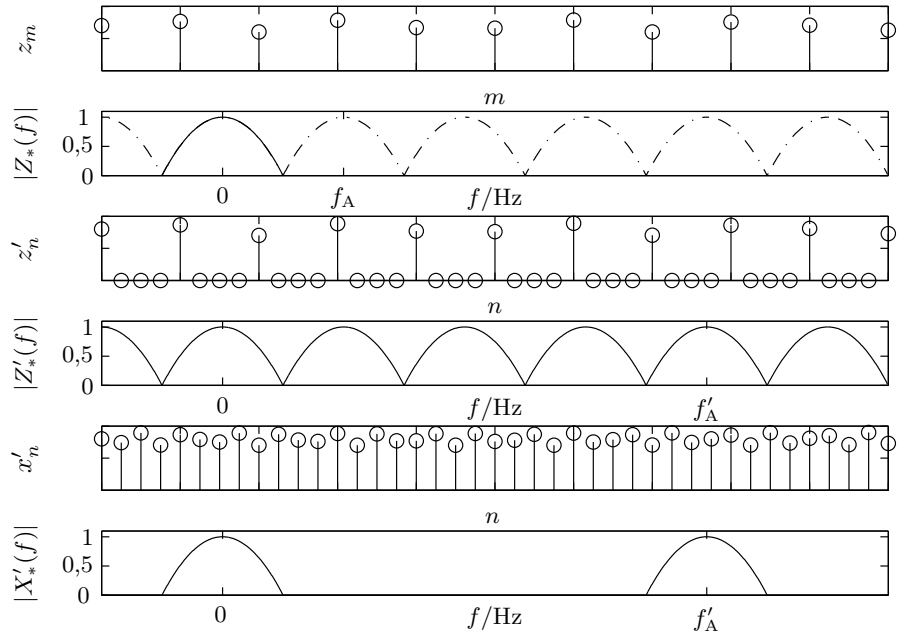


Figure 2.22. Upsampling steps (time and frequency) - Adapted from [23]

2.2.10 Median filter

The median filter is well suited for filtering outliers in a signal and is traditionally used in image processing applications e.g. to filter “salt and pepper” noise [26]. It is a nonlinear filter hence has no associated transfer function. Each sample in a signal is replaced by the value that is obtained by sorting the surrounding samples in a window of width w by their value and taking the middle value of this sorted batch. Outliers are all at the edges of the sorted batch and are thus never picked. If the window has an even value, then the mean of the two middle values is used. Values that are beyond the end points of the signal are considered to be zero.

2.2.11 Wavelet Transform

The Wavelet transform is a signal transformation that has a better time resolution at higher frequencies and a better frequency resolution at lower frequencies compared to the Short Time Fourier Transform. For a signal $x(t)$, it is defined by

$$W_x^\Psi(a, b) = \langle x(t), \Psi_{a,b}(t) \rangle_t = \frac{1}{\sqrt{|a|}} \int_{-\infty}^{\infty} x(t) \Psi^* \left(\frac{t-b}{a} \right) dt \quad (2.59)$$

Where $\Psi_{a,b}(t)$ is the scaled and shifted analysis wavelet, a is the scaling factor and b describes the time shift. A more convenient representation is the description as a function of frequency and time:

$$W_x^\Psi(\tau, f) = \sqrt{\left| \frac{f}{f_\Psi} \right|} \int_{-\infty}^{\infty} x(t) \Psi^* \left(\frac{f}{f_\Psi} (t - \tau) \right) dt \quad (2.60)$$

There is a huge amount of different Wavelets available and a rather complex task is the selection of the right Wavelet for the certain application. Often the right Wavelet is found by trial and error or simply by experience. The presentation of all the different wavelets is far beyond the scope of this thesis so only the used one is introduced in section 4.3.1.15.

Section adapted from [23].

2.2.12 Discrete Wavelet Transform

The Discrete Wavelet Transform (DWT) is the discrete time equivalent to the Wavelet Transform for continuous time signals. For a discrete time signal $x(n)$ it is

$$W_x^{\Psi}(k, m) = \sum_{-\infty}^{\infty} x(n) \cdot 2^{-\frac{k}{2}} \Psi(2^{-k}n - m) \quad (2.61)$$

where the scaling and shifting parameters a and b are in a dyadic scale. This leads to a time frequency resolution grid as seen in

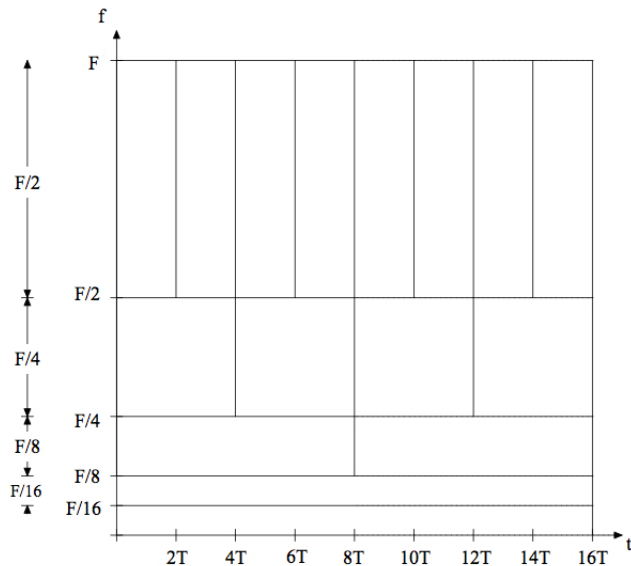


Figure 2.23. Dyadic time-frequency scale of the DWT with the maximum Frequency in the signal F and the sampling time T . (adapted from [23])

Section adapted from [23].

2.2.13 DWT expressed as Multirate filter banks

The DWT can be interpreted as a recursive filtering of the signal with a band- and low-pass filter in each step. The approximate and detail coefficients are calculated by filtering the signal with band- and low-pass filters and a successive downsampling by a factor of 2 (fig. 2.24 illustrates this).

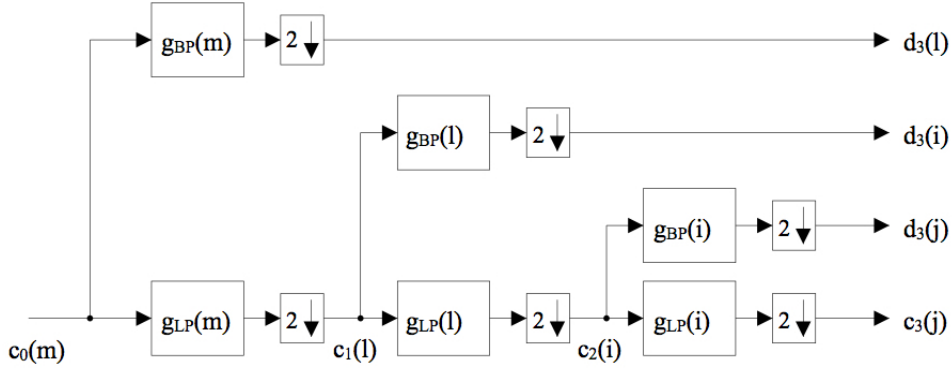


Figure 2.24. DWT expressed as a multirate filter bank (adapted from [23])

This interpretation allows frequency bands to be mapped to the approximate and detail coefficients. For example the first level coefficients describe the upper and lower frequency bands. The first approximation coefficient, which is generated by the low-pass filter describes all frequencies below $F/2$ and the detail coefficient, generated by the band-pass filter describes the frequencies between F and $F/2$. On the next level the low-pass signal is filtered again with the same filters so the lower frequency band is further split.

3

State of the art

3.1 EDR

The influence of respiration on the ECG has been reported as early as 1967 in [14]. [15] describes the influence on the QRS complex and the baseline finding that the baseline is only little affected by respiration. To remove the baseline [27] suggests a method using two consecutive median filters of different window lengths. An EDR method based on statistical properties like the kurtosis of the ECG signal has been developed in [28]. In [29] the PCA is used to derive a respiratory signal from PCAs of different parts of the beat with the signal generated from first PC of the QRS complex performing best. The variability of amplitude and duration of all ECG waves caused by respiration in each lead is quantified in [17] leading to the conclusion that respiration is only visible in certain leads. A comparison of different methods including a wavelet based one has been done in [30] with the result that the wavelet method does not perform well compared to a RR based method or a simple bandpass. Wavelets have also been used in [31] with similar results. EDR based on RSA has been examined in [13] that suggests that there is a link between the respiration and the RSA but there are many other influences that also change the heart rate. The hypothesis that RSA decreases with higher age could not be verified in this paper. It even showed an inverse proportionality.

3.2 TWA

The role of Ca^{2+} on the genesis of TWA has been proposed in [10]. A more complete overview of the role of Ca^{2+} along with extensive review of the usefulness of TWA for predicting sudden cardiac death is conducted in the meta

study paper [32]. A link between cardiac fibrillation and TWA is established in [11] by looking at the cellular level and examining the influences on the ECG. In [8] different preprocessing stages have been tested with the spectral method and a time domain method with the result that the preprocessing can influence the detection results significantly. The problem of the TWA definition is also mentioned here. The influence of the heart rate on TWA has been investigated and confirmed in [9]. An implementation of the spectral method including the introduction of a significance estimation with the K-score is proposed in [33]. The method was tested under resting and controlled exercise condition where alternans was a statistically significant predictor of ventricular vulnerability only during exercise condition. Periodic Component Analysis as a method for signal processing in speech has been proposed in [34]. The application of Periodic Component Analysis in ECG signal processing in particular to separate maternal from fetal ECG recordings has been done by [24]. This method has been adapted for detecting TWA in [25] and found to be superior in performance than other methods.

4

Methods

4.1 Datasets

In this section all datasets used in this thesis are listed. For EDR two datasets have been used and for TWA one dataset. All datasets are publicly available on the Physionet website [35].

4.1.1 MIT-BIH Polysomnographic Database (slpdb)

This database has been selected for the EDR methods because it contains, among others, an ECG channel and one respiratory channel. The recordings have a duration between 2 and 7 hours depending on the subject. It contains 18 recordings from 16 different subjects that have been sampled with a sampling rate of $f_s = 250$ Hz. [36]

4.1.2 Fantasia Database (fantasia)

This database is also used for the EDR methods. It contains 40 recordings of healthy subjects of two age groups, 20 younger and 20 elderly ones. Both ECG and a respiratory signal have been recorded for all records and were digitized with a sampling rate of $f_s = 250$ Hz. The subjects were watching the movie “Fantasia” lying in a supine position during recording. [37]

4.1.3 T-Wave Alternans Challenge Database (twadb)

This database was generated for the “PhysioNet/Computers in Cardiology Challenge 2008” in which different T-wave alternans algorithms had to be developed. It consists of 100 short multichannel ECG recordings with 2 channels (16 subjects), 3 channels (12 subjects) and 12 channels (72 subjects). The recordings are mixed real ECGs from other databases and synthetic ones

with and without artificially added alternans. All signals have been resampled to a sampling frequency of $f_s = 500$ Hz. After the challenge, a ranking was released that gives the order of the amount of alternans in the recordings. However, this ranking has been generated from the results of the participating teams of the challenge which can be a problem. The absolute amplitude of the alternans in each recording is not given since for some of them, especially the real ECG signals, the value is not known. This groundtruth is only known for the signals with artificially added alternans but is not published. [38]

4.2 Signal conditioning and filtering

The raw ECG signals contain various forms of noise which have to be removed prior to any signal processing.

4.2.1 Baseline wander removal

The relevant part of an ECG signal is only the voltage swing around the isoelectric line (the baseline). The potential to which the ECG signal is measured against is not constant and thus its amplitude can change magnitudes larger than the relevant parts of the signal itself. This offset is referred to as the baseline wander. Fortunately, these changes are typically much slower than the changes in the ECG signal. Baseline wander noise mainly consists of low frequencies but it overlaps with the relevant spectrum of the ECG signal, especially at the part around the respiration frequencies between 0.17 and 0.83 Hz. In this thesis, a high-pass filtering method and a median filtering method have been tested. The high-pass technique is a well known and easy to implement method. The ECG signal is filtered with a high-pass filter with a cut-off frequency around $f_c = 0.1$ Hz.

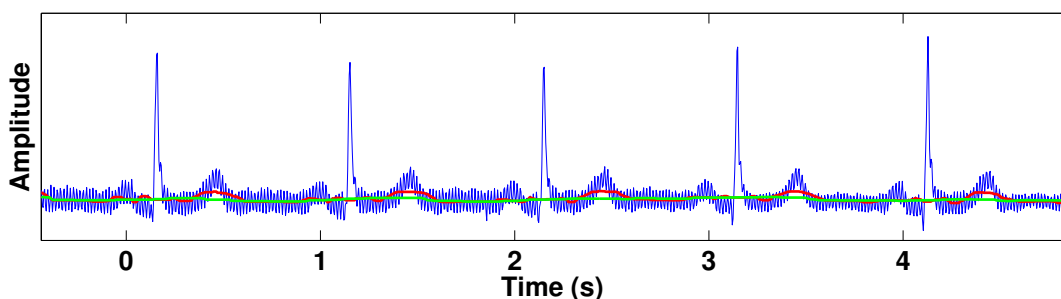


Figure 4.1. Original ECG signal (blue), 200 ms median filtered (red), 200 ms and 600 ms median filtered (green)

The second method uses two median filters. The ECG signal is first filtered by a median filter with a window size of 200 ms which removes the QRS complex and the P wave. The resulting signal is then again filtered by a median filter of 600 ms which removes the remaining T wave resulting in the estimated baseline. This baseline is then subtracted from the original ECG to get the baseline removed ECG signal [27]. The process is illustrated in fig. 4.1 where the green signal is the baseline that is then subtracted from the original ECG signal in blue. This method shows good performance for short and high disturbances higher than the signal itself and also for slow varying baselines (see fig. 4.2). In addition to that, this method does not disturb clinically valuable data in the ST segment like ST elevation or depression (see fig. 4.3). In the frequency domain this method only removes energy in the frequencies below 2 Hz and leaves the higher ones mostly untouched (see fig. 4.2). After visual inspection the median filter method has been chosen because of its excellent performance in various conditions.

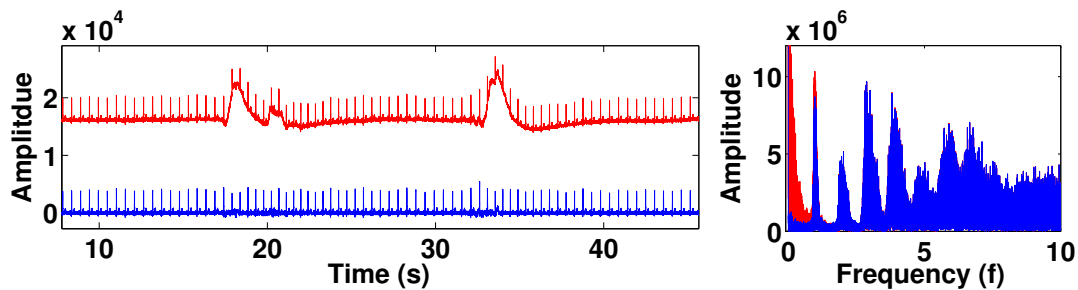


Figure 4.2. Original signal (red), baseline removed signal (blue) in time- (left) and frequency-domain (right))

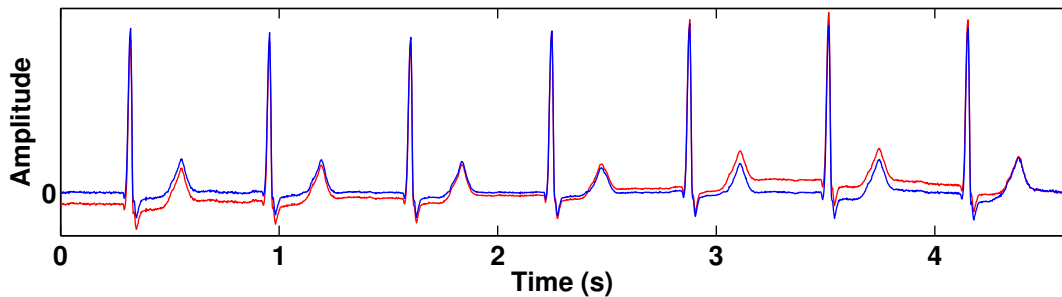


Figure 4.3. Original ECG signal (red), median filtered signal (blue) - no visible ST distortion

One disadvantage of this method is its long computation time because the values have to be ordered for every step to obtain the median value. This is computationally expensive especially for large windows e.g. 600 ms. Estimating the baseline of a 2 hours signal recorded with a sampling frequency of 250 Hz takes for example about 13 s compared to a simple low-pass filtering which takes about 2 s.

4.3 ECG derived respiration (EDR)

The goal of ECG derived respiration is to generate a continuous respiratory signal from one or more ECG leads. In such a signal, a positive flank corresponds to inhalation and a negative one to exhalation. In this thesis several different methods were implemented and compared with each other. In addition to that, a method was developed to combine the different single methods to get a more robust estimation of the EDR signal. The general approach is to extract various properties or points out of the signal from which the EDR signal is then generated.

4.3.1 Single lead EDR methods

This section describes methods that use the signal of only one electrode to generate an EDR signal. For the methods to work it is essential that the signal is properly selected because respiratory information is only available in certain leads.

4.3.1.1 Normalization of the EDR signals

Since each of the different EDR methods generates signals with arbitrary amplitude swing, all signals are normalized for easier comparison. All of the methods contain some sort of post filtering so it is assumed that the signal amplitudes are within a certain deviation without large outliers. Therefore the signals are normalized based on their standard deviation. First the STD of the total signal is calculated and each signal value is then divided by this STD resulting in signals with a $STD\{s(t)\} = 1$.

4.3.1.2 Fiducial point detection

To detect all fiducial points the methods developed by Lenis have been used [39]. In this thesis the fiducial points could be detected with a correct rate of

97,87% with a sensitivity of 90,59%. Several works in addition to this have contributed to the development of a toolbox for the Institute of Biomedical Engineering at KIT that has been used in this work. This toolbox is capable of detecting all major fiducial points ($Q, R, S, T_{on}, T, T_{off}$) and in addition to that is able to detect and classify ectopic beats and artefacts.

4.3.1.3 R peak

This is a QRS complex based method that uses the amplitude of the R point as a data source for extracting an EDR signal. The method is comparable to the classical upsampling of a signal with some exceptions. First, an empty signal with the same length as the ECG signal is generated. Then all values at the R-peaks are copied to the empty signal which results in a series of impulses at the locations of the R peaks. This can be interpreted as sampling the ECG signal with a non-constant sampling frequency that varies with the RR-interval $t_{RR}(n)$ and adding a variable number of zeros in between. The mean is subtracted to get a signal that is oscillating around the zero line (fig. 2.22). The last step is the interpolation with a low-pass filter. For faster computation, a 10-order Butterworth filter without phase distortion (resulting in a 20-order Butterworth filter after phase compensation) is used as a replacement for the ideal low-pass filter. The sampling frequency f_A is approximated by the reciprocal of the mean RR-interval \bar{t}_{RR} of the signal which can be seen as the sampling frequency of the impulse series.

$$f_{nyquist} = \frac{f_A}{2} = \frac{1}{2 \cdot t_A} \approx \frac{1}{2 \cdot \bar{t}_{RR}} = f_c \quad (4.1)$$

After normalization (see section 4.3.1.1) the resulting signal is the EDR signal. Using this method in contrast to e.g. spline interpolation was chosen because spline interpolation introduces extra frequency content especially at higher frequencies whereas this method does not. Therefore this method can be regarded the most conservative one because no additional information is added to the signal.

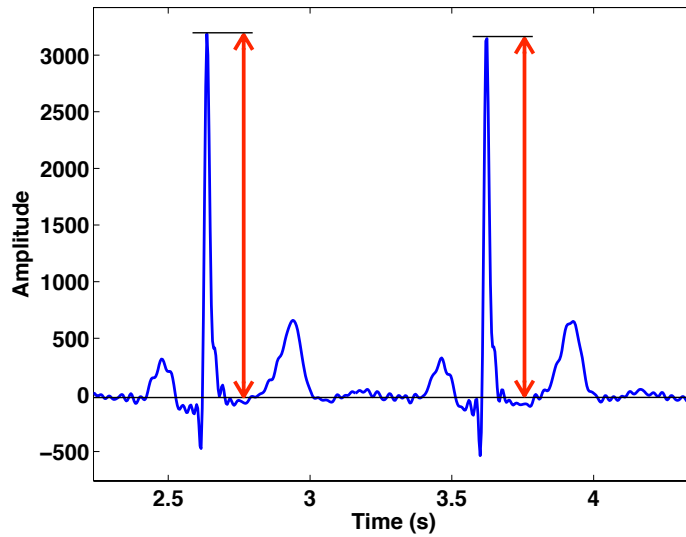


Figure 4.4. R-peak amplitude method

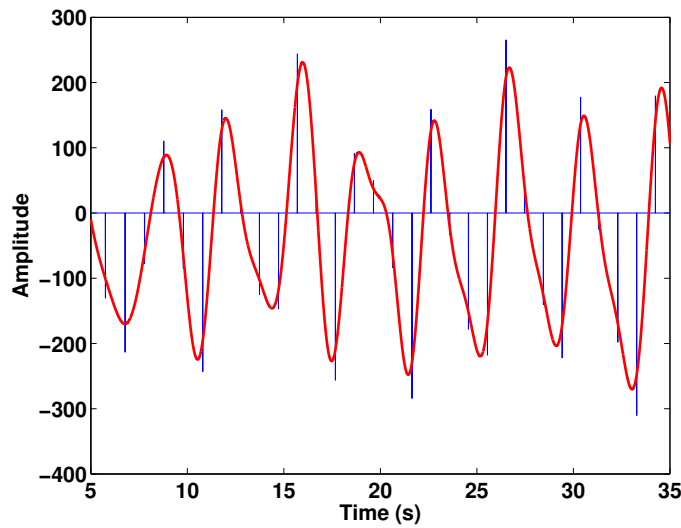


Figure 4.5. Impulse series (blue), low-pass filtered (and amplified for better visibility) impulse series (red)

4.3.1.4 T peak

The T peak method is similar to the R-peak method but uses the detected T peak for the impulse series. Although studies show that the amplitude of the T wave is less affected by the modulation than the QRS complex, [17]

this and all other T wave methods are used because they deliver information from a different point in time than the ones working on the QRS complex. For a later combination of the signals this can be beneficial.

4.3.1.5 QRS integral

This method is similar to the R peak method. The difference is the way the impulse series is generated. For the height of the impulses the integral over a fixed window centred around the detected R peak is used while for the location of the impulses in the new signal, the R points are used. The window size is calculated from the mean period between the Q and S points. This ensures that the window is best adapted to different datasets. Interpolation is performed the same way as in the R peak method.

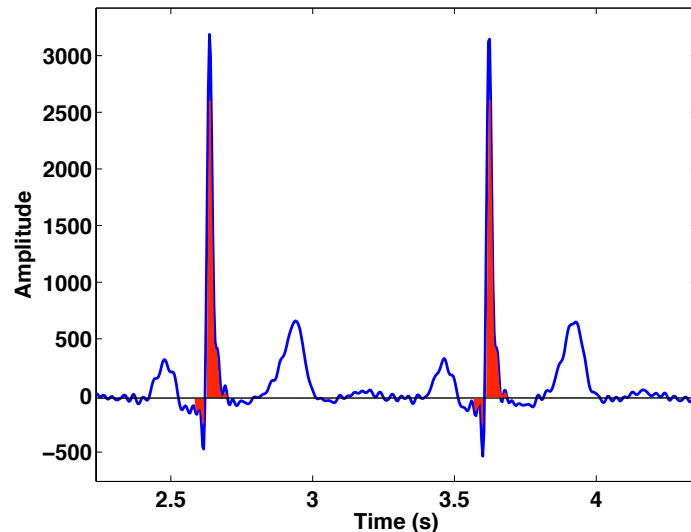


Figure 4.6. QRS Integral method

Compared to the R peak method, this one should be more robust against additive mean free noise which is averaged out by integration. The prerequisite is a correct detection and removal of the baseline because deviations are added up by the integration. If the deviations are small compared to the signal, this error is also small. This is valid for the R point but is not necessarily for the areas around the Q and S points. The reason being these points are situated closer to the isoelectric line and thus have smaller signal values. Therefore, a correct baseline removal is required.

4.3.1.6 T integral

The difference between this method and the QRS integral method is the use of the detected T peak instead of the R peak. The window size is calculated by the mean difference between the detected T wave start and end points of all waves.

4.3.1.7 QRS width

This method uses the duration between the Q and S points as the values for the impulse sequence. A major problem for this method is its dependence on the precise detection of the Q and S points which is difficult not only for algorithms but even for physicians.

4.3.1.8 QR slope

In this method the maximum inclination between the Q and R points is used as a value for the impulse series. The method was also introduced with the intention of testing if other features of the QRS complex, like the slope, are possibly better suited than the common R peak.

4.3.1.9 T slope

Instead of the slope between the Q and R points in the QR slope method the slope between the T wave starting point and T peak point is used.

4.3.1.10 RT peak

In this method the feature for the impulse series is the difference of the R and T amplitudes. This is also a new feature that was introduced to investigate other QRS complex features. The motivation for choosing the difference between the two peaks arrived from two ideas:

First the independence of the baseline because it is contained in both amplitudes. A constraint is the assumption that the baseline does not change between the R and T wave. Tests with and without removed baseline have shown that the baseline removal is still beneficial and leads to better results what means that the assumption of a slowly varying baseline is not valid.

The second idea of this method is to eliminate varying intensities of the modulation. Since the amplitude of the modulation at a given beat is approximately the same at the QRS complex and the T-wave but can vary over a

timespan of several beats the amplitude of the EDR signal also changes over time. To overcome this issue the ratio of the modulations is used by taking the difference between the R and T amplitudes. This works because of the different amplitudes of the QRS complex and T-wave especially in the ECG lead II. However, the smaller the difference between those maximum amplitudes is, the worse this method should work because the signal to noise ratio is reduced assuming a constant noise level.

4.3.1.11 RR interval

The RR interval method is based on the respiratory sinus arrhythmia (RSA). First, all RR intervals are calculated and the value is placed in an empty signal at the point in the middle between two R peaks. Then the impulse series is interpolated like in the R peak method section 4.3.1.3. The resulting signal has to be inverted to correlate with the traditional respiratory signal because during inhalation the heart rate increases and the RR intervals get shorter so the signal decreases as the lungs fill with air whereas during exhalation the signal increases. There was no interval correction implemented however only beats classified as normal are used and no ectopic ones. In fig. 4.7 an RR interval EDR signal with an added constant offset is shown to visualize the correlation between the modulation that is used in the R peak method and the RR interval EDR signal.

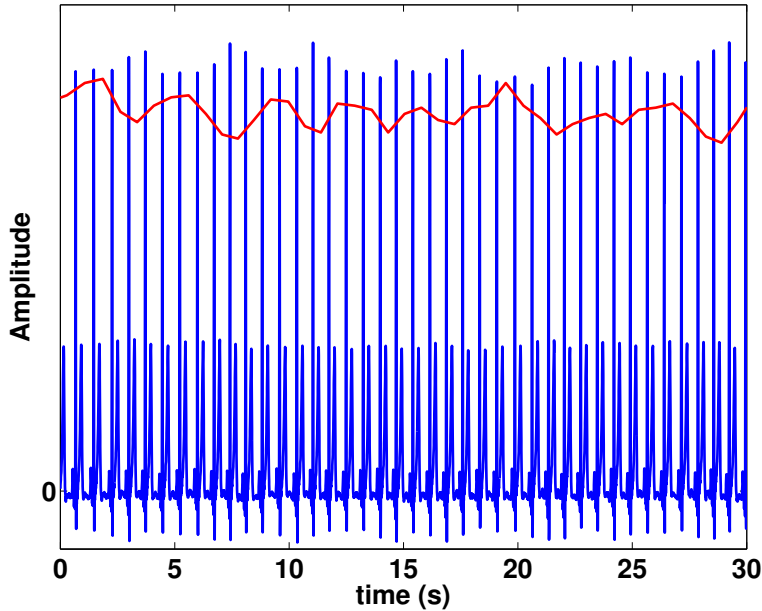


Figure 4.7. original ECG signal (blue), interpolated RR interval signal (red) with added offset to visualize correlation with modulation

4.3.1.12 PCA

In [29] the PCA method has been applied to different parts of the ECG beats with the result that using only the QRS-complex performed best so this has been implemented in this thesis. First, all QRS complexes are extracted from the ECG signal and placed in a matrix. The QRS complex is defined as the 120 ms long area 60 ms left and right of the detected R point. Each QRS complex is an observation of a vectorial random variable. So, in equation (2.44) the vector \mathbf{x} turns into a matrix because each observation x_n is one QRS-complex.

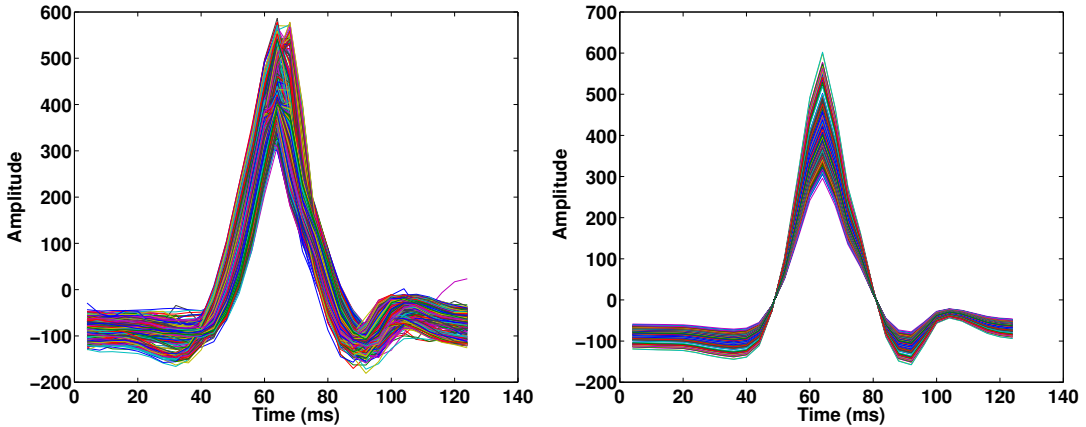


Figure 4.8. Projection of the coefficients obtained by a PCA from the QRS complexes onto the first score

The coefficients of the first principal component (PC) are chosen for forming the impulse series like in the R peak method. Since the assumption that the largest alteration of the QRS complex is done by the respiration the first PC is chosen. The not centred PCA is used so the first PC represents the deviation of each QRS complex from the mean QRS complex.

4.3.1.13 RS Amplitude

This method is similar to the R peak method but instead of the amplitude of the R peak the difference between the amplitudes of the R and S peaks are used to generate the impulse series which is interpolated to get the EDR signal. Since the measurement of the amplitude is not done against the isoelectric line this method is independent of any baseline wander. A problem with this method is the difficulty to accurately detect the S point.

4.3.1.14 Kurtosis

A method that uses statistical properties like the kurtosis of an ECG signal has been proposed in [28]. This method uses all values of the signal between two consecutive R peaks. From those values the Kurtosis is generated and used as a sample point for the EDR signal at the position of the second R peak. This results in an impulse series which is interpolated to get an EDR signal. The method has been chosen because it uses the higher order statistics of the whole ECG signal.

4.3.1.15 Discrete wavelet transform

The wavelet method has been adapted from [31] and [30]. The idea of the method is to decompose the ECG signal and then reconstruct it using only the detail coefficients representing the frequency range of the respiration (below 0.5 Hz). When using a signal with a sampling frequency of 250 Hz this corresponds to the detail coefficients 9 and 10 (see equation (4.2), equation (4.3) and fig. 4.9).

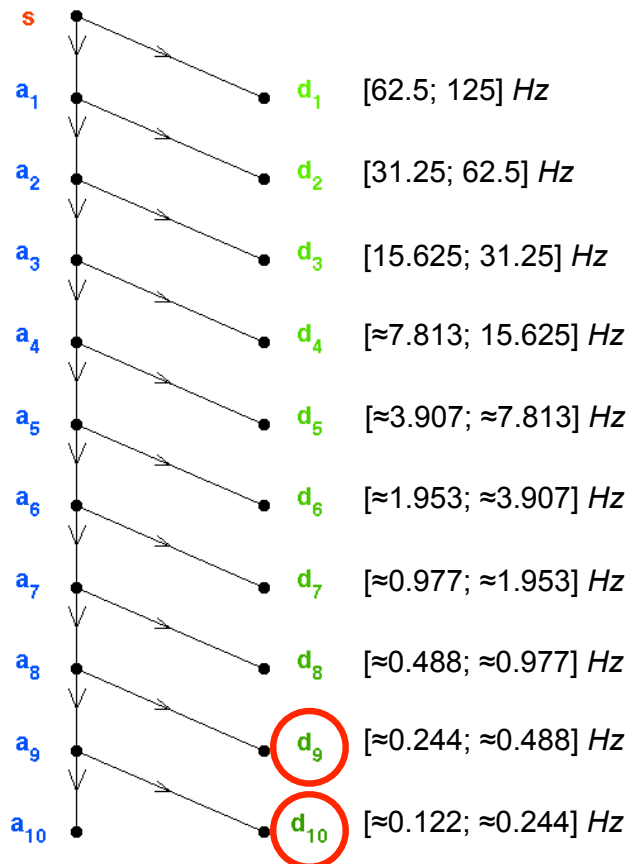


Figure 4.9. Scaling function (red) and wavelet function (blue) of the biorthogonal 5.5 wavelet

For this method it is important not to destroy the information by the signal preprocessing stages especially the baseline correction because the information is extracted from there so the raw ECG signal without preprocessing is used. All filtering is already done by only using certain coefficients.

$$f_{max_{d9}} = \frac{f_s}{2^n} = \frac{250 \text{ Hz}}{2^9} \approx 0.49 \text{ Hz} \quad (4.2)$$

$$f_{max_{d10}} = \frac{f_s}{2^n} = \frac{250 \text{ Hz}}{2^{10}} \approx 0.24 \text{ Hz} \quad (4.3)$$

The biorthogonal spline wavelets (“bior 5.5”) have been used like in [30] and is commonly found in literature to analyse ECG signals.

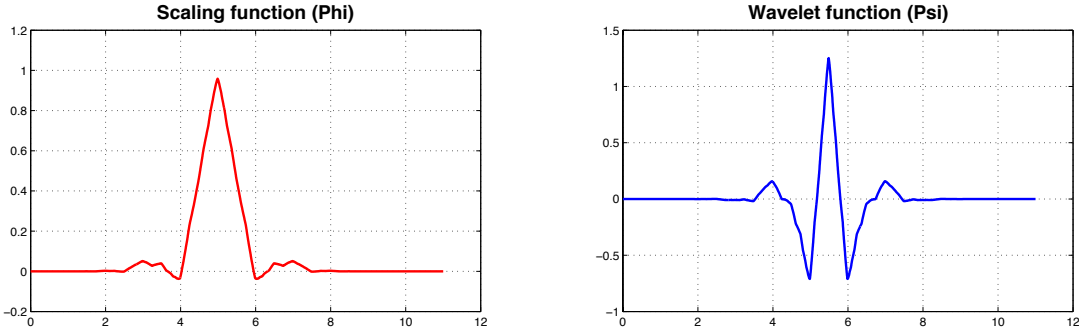


Figure 4.10. Scaling function (red) and wavelet function (blue) of the biorthogonal 5.5 wavelet

A sample EDR signal generated with this method is pictured in fig. 4.11. More sample signals generated by all methods for the same interval can be seen in fig. 4.23.

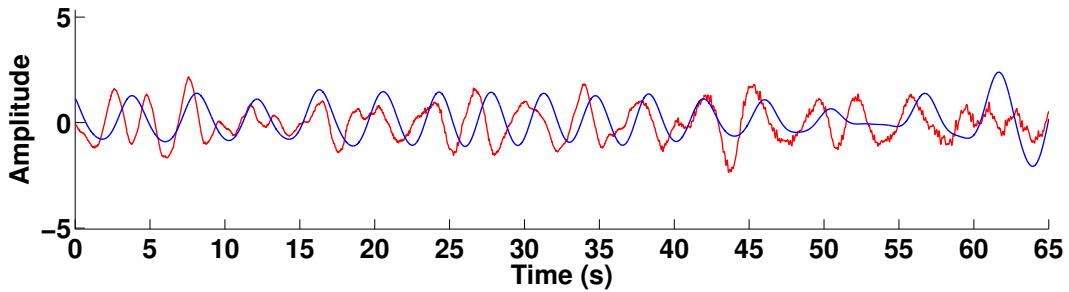


Figure 4.11. reference respiratory signal (blue), wavelet EDR signal (red)

4.3.2 Comparison of all methods

To be able to rate their individual performance, all methods are compared with each other. Comparison is done against a reference respiratory signal that has been recorded by traditional methods. These signals also contain noise, mainly a baseline wander and some HF noise. To remove the baseline from the measured respiratory signal, an approach with a median filter similar to the baseline removal of the ECG has been chosen. Since the breathing signal has

only one pattern unlike the ECG signal which has a short QRS complex and longer P and T waves, only one median filter has been used with a window size of 6 s what is approximately the duration of the slowest possible breathing period of $T_{breath_{max}} = 5.88$ s.

$$T_{breath_{max}} = \frac{1}{f_{breath_{min}}} = \frac{1}{10 \text{ min}^{-1}} \approx 5.88 \text{ s} \quad (4.4)$$

The filtered signal is the baseline and is subtracted from the original signal to get a baseline free signal. This has been determined to give the best performance for removing slow and fast varying baselines (see fig. 4.12).

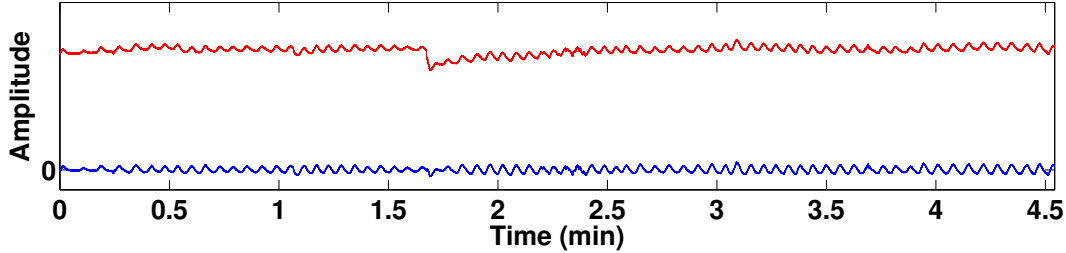


Figure 4.12. original respiratory signal (blue), median filtered (6 s window) original respiratory signal (red)

In all EDR methods a high-pass filter is used to remove the offset induced by the methods themselves. For better comparison this filter is also used for the measured signal in addition to the median filter.

4.3.2.1 Benchmark functions

For comparing the measured respiratory signal to the EDR signal, three different methods have been implemented:

- Number of peaks (time domain method)
- Respiration rate (frequency domain method)
- Cross-correlation/Cross-covariance (X-Corr/X-Cov)

The benchmark was carried out on non overlapping windows of the signal with a width of 20 s. The score of the benchmark for all three methods is a value between 0 and 1 where 1 is the best possible score. These scores are not comparable between two benchmark methods but only within the same. For

instance, this implies that the score of the cross-correlation benchmark can not be compared with that of the peaks benchmark.

4.3.2.2 Number of peaks

For the number of peaks method, all peaks in the signals in the time domain are counted with a minimum distance between them of $T_{peakdistance} = 1\text{ s}$. This is about 15% less (see equation (4.6)) than the fastest breathing period (see equation (4.5)) to avoid high numbers caused by interpolation artefacts. Peaks that occur after a peak inside this minimum window of 1 s are ignored.

$$T_{breath_{min}} = \frac{1}{f_{breath_{max}}} = \frac{1}{50\text{ min}^{-1}} \approx 1.2\text{ s} \quad (4.5)$$

$$T_{peakdistance} = T_{breath_{min}} \cdot 85\% = 1.02\text{ s} \approx 1\text{ s} \quad (4.6)$$

This method has a higher temporal resolution than the respiration rate method described in section 4.3.2.3.

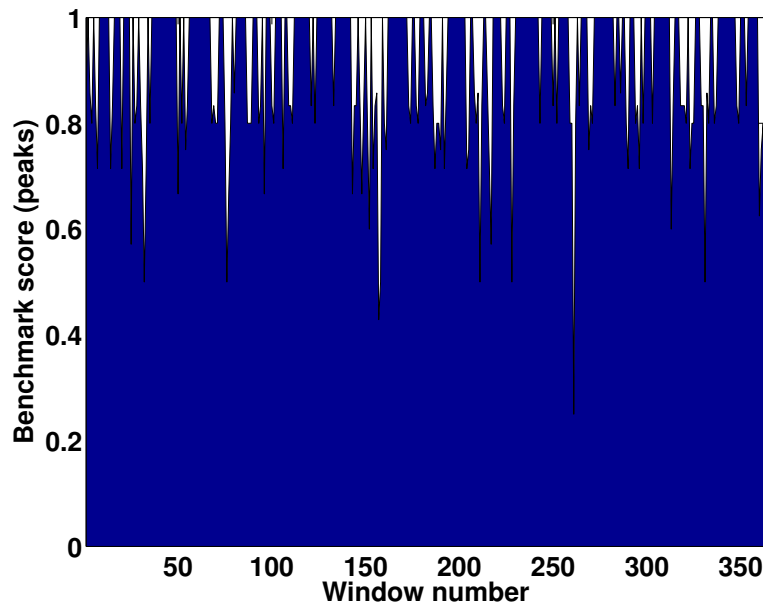


Figure 4.13. Sample peaks benchmark for one signal of the fantasia database (median score: 0.93)

4.3.2.3 Respiration rate

The respiration rate is determined with the help of the power spectral density estimate calculated by Welch's method. The FFT size is calculated in a way that a minimum resolution of 0.5 min^{-1} is achieved. The window size for the Welch estimate is set to 10 s with a 90% overlap. So in each 20 s long benchmark step, the averaged spectrum is generated by 10 single spectra. We assume the peak of the Welch spectrum is the respiration frequency in the observed 20 s.

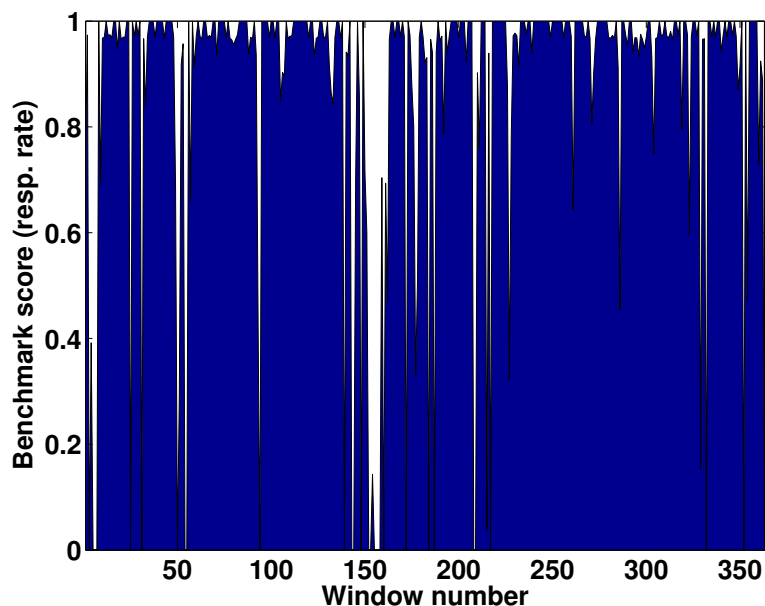


Figure 4.14. Sample respiration rate benchmark for one signal of the fantasia database (median score: 0.97)

4.3.2.4 Cross-correlation/Cross-covariance

This benchmark method is the strictest of all because the correlation is a direct measurement of the similarity of two signals [40]. For the score of the benchmark, the maximum of the normalized cross-covariance of a maximum shifting of $\tau_{max} = 10\text{s}$ is used. The shifting is granted because some methods might produce an EDR signal with a slight phase shift. The phase shift can be tolerated because it does not change the quality of the signal for applications like determination of the respiration rate. The normalization is performed in a way that the auto-correlation of the signals at a lag of 0 are equal to 1 ($r_{xx}(0) = 1$).

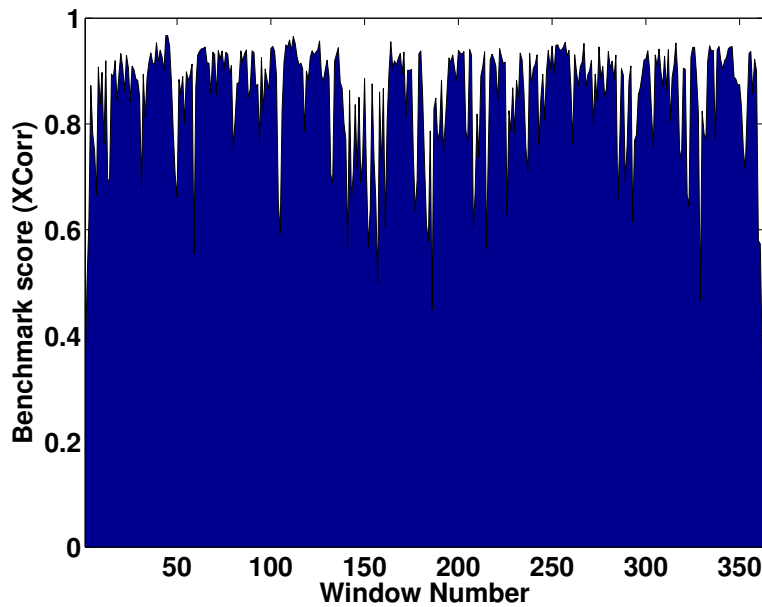


Figure 4.15. Sample xcorr benchmark for one signal of the fantasia database (median score: 0.87)

4.3.2.5 Possible error sources

There exist several error sources that can influence the benchmarking process. One of them is a noisy ECG signal from which it is not possible to reconstruct an EDR signal with any method. In addition, the reference respiratory signal can also contain noise. In this case, the EDR signal can even have a better quality. Unfortunately, it is not possible to detect those errors automatically, so an EDR signal has to be always inspected alongside the ECG signal in order to be at least able to sort out errors due to poor ECG signals. Errors in a reference signal can only be detected by visual inspection. In this thesis it was not possible to inspect and annotate several hours of respiratory and ECG signals so these error sources are only mentioned here for the sake of completeness but are not eliminated.

4.3.2.6 Results

For the evaluation of the performance, each signal of one dataset is first analysed in non-overlapping windows of 20 s resulting in a series of performance values. To exclude signal parts of bad quality, a final benchmark value is generated by taking the median value of all 20 s windows. So for each signal there is exactly one benchmark value per benchmark method. The evaluation has been carried out on the “Fantasia” dataset with the results for the Xcorr

benchmark seen in fig. 4.18, the respiration rate score in fig. 4.17 and the peaks score in fig. 4.16.

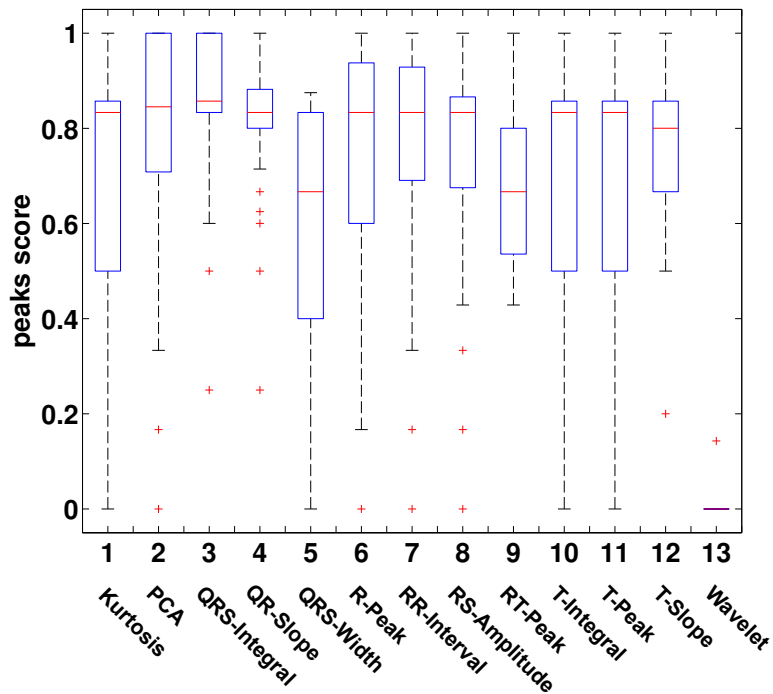


Figure 4.16. Number of peaks benchmark of all EDR methods on “Fantasia” dataset

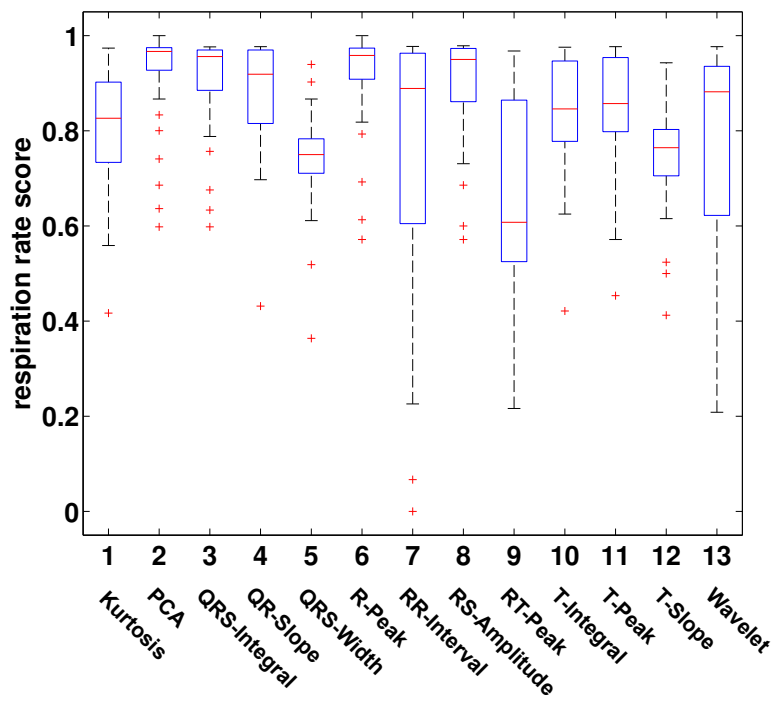


Figure 4.17. Respiration rate benchmark of all EDR methods on “Fantasia” dataset

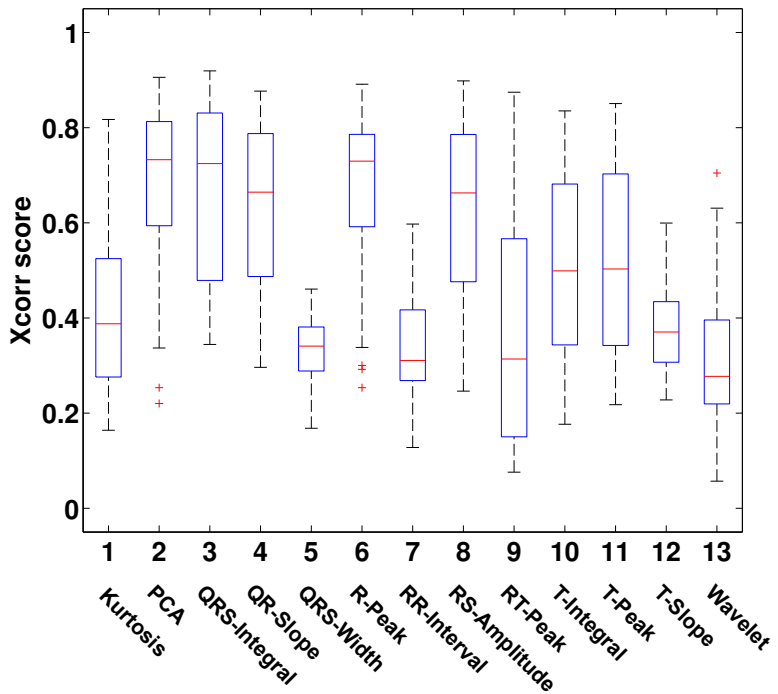


Figure 4.18. Xcorr benchmark of all EDR methods on “Fantasia” dataset

The benchmark ordered by the median Xcorr (see table 4.1) provides a clue as to which method works best. However not only the median that is important but also the interquantile distance (25%-75%) since the latter indicates the robustness of a method. The smaller the interquantile distance, the robuster the method is.

Method	Median	i.q. dist. (25%-75%)
PCA	0.733	0.2189
R-Peak	0.730	0.1941
QRS-Integral	0.724	0.3520
QR-Slope	0.664	0.3006
RS-Amplitude	0.663	0.3096
T-Peak	0.503	0.3607
T-Integral	0.499	0.3380
Kurtosis	0.388	0.2489
T-Slope	0.370	0.1274
QRS-Width	0.341	0.0925
RT-Peak	0.314	0.4164
RR-Interval	0.311	0.1484
Wavelet	0.277	0.1764

Table 4.1. Ordered Xcorr benchmark results on “Fantasia” database

The method based on wavelet decomposition does not seem to work well. Other studies using this method drew similar conclusions [30],[31]. The correlation of the T wave methods are performing worse than the ones on the QRS complex. This could be related to the worse signal to noise ratio since the amplitude of the T wave is much lower than the one of the QRS complex but the noise is the same at every point of the signal. The RR interval method seems to be an unreliable method as well which confirms the presumption in section 2.1.7. The PCA based method on the QRS complex is performing best and is closely followed by the R peak.

4.3.3 Signal fusion

The next step for improving the performance of the single methods is combining them in a way that the combined signal performs better than each of them separately. In this thesis a linear approach is used which means that the

single EDR signals are linearly added to obtain a new signal. The idea behind this is that each of the single signals contains added random noise. By adding these signals the signal is amplified by constructive interference while the noise gets cancelled out by destructive interference. The linear combination can be expressed as

$$s_{ideal}(t) = \mathbf{s}(t) \cdot \mathbf{a} = [s_1(t) \ s_2(t) \dots s_n(t)] \cdot \begin{bmatrix} a_1 \\ a_2 \\ \vdots \\ a_n \end{bmatrix} \quad (4.7)$$

with the signal vector containing all single EDR signals

$$\mathbf{s} = [s_1 \ s_2 \dots s_n] \quad (4.8)$$

and the combination vector (also denoted as parameter vector or weighting vector) that defines how much each of the single EDR signals is contributing to the combined signal

$$\mathbf{a} = [a_1, a_2, \dots, a_n]^T \quad (4.9)$$

The vector \mathbf{a} is constant but is yet to be determined. For the signal to noise ratio this can be expressed in a model (for better readability restricted to two signals). The combined signal can be expressed as a summation of the two input signals $x = s + n_x$ and $y = s + n_y$ where s is the signal, n_x and n_y are the noise terms.

$$z = ax + by = s + n_x + s + n_y = (a + b)s + an_x + bn_y \quad (4.10)$$

For the power densities this becomes

$$\sigma_z^2 = a^2\sigma_x^2 + b^2\sigma_y^2 = (a^2 + b^2)\sigma_s^2 + a^2\sigma_{nx}^2 + b^2\sigma_{ny}^2 \quad (4.11)$$

This leads to the SNR

$$SNR_z = \frac{a^2\sigma_x^2 + b^2\sigma_y^2}{a^2\sigma_{nx}^2 + b^2\sigma_{ny}^2} \quad (4.12)$$

When choosing a and b optimally such as $a = 1/\sigma_{nx}$ and $b = 1/\sigma_{ny}$ equation (4.12) becomes

$$SNR_z = \frac{1}{2} \left(\frac{\sigma_s^2}{\sigma_{nx}^2} + \frac{\sigma_s^2}{\sigma_{ny}^2} \right) = \frac{1}{2} (SNR_x + SNR_y) \quad (4.13)$$

4.3.3.1 Optimal parameter vector for combination

To find out if a combination of EDR methods is able to achieve a better performance than a single method, an optimal parameter vector \mathbf{a} in equation (4.7) has to be found. In the first step this optimal parameter vector is found for each subject in the “Fantasia” dataset. To speed up the optimization and remove methods with low quality during development, the EDR signal count has been restricted to 6 signals. This means that out of the 13 implemented methods only 6 had to be chosen. The choice included the three best performing methods (PCA, R-Peak and QRS-Integral) along with the RS Amplitude method, which is independent of baseline wander, and the two best methods of the T wave because they contain information gathered from a different point in time than the QRS complex methods. For identifying the optimal parameters, it is necessary to have valid EDR signals and generating valid EDR signals requires a clean ECG signal without any major disturbances. Therefore only 10 min long parts of each subjects’ ECG without visual disturbances have been manually selected to remedy some of the issues mentioned in section 4.3.2.5. In the algorithm all 6 EDR signals are generated and aligned so there is no phase difference between them. This is necessary because the different EDR methods can generate signals with slight phase differences. The aligning is done by calculating the maximum cross-correlation between each EDR signal with the first EDR signal (in this case the one from the PCA method), allowing only a shifting of less than 5 s and is followed by aligning it. After that, all signals are aligned to the first EDR signal. The borders of the signals are now different so all signals are cropped. There is hence a value of each signal at every point in time, that means the resulting EDR signal has always the same or a shorter length than the ECG signal. In addition to that, the signals are multiplied by -1 if the cross-correlation is negative. This is necessary because some methods might generate an inverted EDR signal depending on the shape of the ECG signal. An example is a negative T wave compared to a positive QRS complex which leads to an inverted signal of the T peak method compared to the R peak method.

For finding the optimal parameter vector \mathbf{a} , MATLAB®'s built in optimization functions are used. Restrictions for the parameter vector are that all coefficients have to be positive because otherwise there would be destructive interference of the signal. An additional condition is that the sum of all coefficients for one signal have to be one so the total signal has a comparable amplitude to the single methods. Three different algorithms have been used: Fmincon (builtin MATLAB®function), LSQ-Nonnegative (builtin MATLAB®function) and LS (least squares problem).

Fmincon is an optimizing algorithm for finding constrained nonlinear minima of multivariable functions. Since the cross-correlation of two signals is a nonlinear function, this kind of optimization algorithm has to be employed. The constraints used for the algorithm are values between 0 and 1 for each coefficient. For the start parameter vector each coefficient has the value 0.5 so each signal is weighted equally at the starting point. Normalization is performed afterwards by dividing each coefficient by the sum of all so the final sum of all coefficients equals 1. The LSQ-Nonnegative algorithm solves a LS problem with the constraint of only positive coefficients. For some signals this approach does not converge and thus has no solution. The third optimization algorithm is a generic least squares approach between the reference respiratory signal and the combined EDR signal. This approach can lead to negative coefficients in the weighting vector and constraints are not possible. This is contradictory to the assumption that the respiratory signal is amplified by the summation of different EDR methods and the noise gets cancelled out by destructive interference. Nevertheless, it is possible that negative values lead to a better combined signal because the noise is incidentally reduced further with these values.

The cross-correlation performance of the three different methods when generating an EDR signal with the optimal parameter vector for each subject in the “Fantasia” database and comparing it to the reference respiratory signal is shown in fig. 4.19. The corresponding data is listed in table A.1, table A.2 and table A.3. The results show only slight differences between the algorithms. The best one is achieved with the LS approach but as mentioned earlier it allows negative values for the weighting vector that leads to destructive interference of the signal which is not desired. The second best result is achieved with the LSQ-Nonnegative approach when ignoring the signals where no solution can be found. Fmincon is very similar in performance to the LSQ-Nonnegative algorithm but includes all subjects of the dataset.

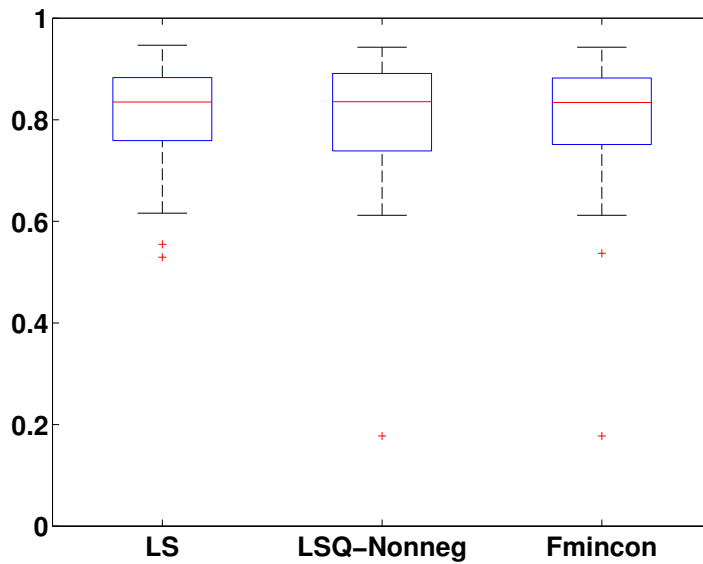


Figure 4.19. Cross-correlation of combined signals and single EDR signals with reference respiratory signal (“Fantasia” database)

4.3.3.2 General parameter vector for combination

To be able to generate EDR signals for subjects where no reference is available, a general weighting vector \mathbf{a} that can be used for every signal has to be found. This general weighting vector is obtained by taking the mean or median of all optimal weighting vectors of each subject from the “Fantasia” dataset. In table A.1, table A.2 and table A.3 all optimal weighting vectors per subject are listed. The mean or median of each column of these three tables leads to table 4.2 for the three different algorithms. The median and mean parameter vector is calculated by using only the valid solutions especially for the LSQ-Nonnegative algorithm, where there is no solution for some subjects.

All three algorithms create similar general parameter vectors with the PCA and QRS Integral method being weighted most (see table 4.2). The T peak signal is also taken into account, however to a lesser extent. The contribution of the three other methods is negligible. An interpretation for that result is that the methods with small coefficients do not contain additional information and hence they are not used. The T peak method is used because it contains additional information even though its general performance is worse than for example the one of the R peak method.

Algorithm	PCA	QRS-Int.	R-Peak	RS-Ampl.	T-Int.	T-Peak
LS (mean)	0.5624	0.3279	-0.1006	0.0615	0.1391	0.0098
LS (median)	0.6523	0.3444	-0.1384	-0.0033	0.0706	0.0744
LSQ-Nonneg. (mean)	0.2671	0.3128	0.0728	0.1099	0.0806	0.1568
LSQ-Nonneg. (median)	0.4120	0.4080	0	0	0.0635	0.1165
Fmincon (mean)	0.2419	0.3113	0.0590	0.1147	0.0751	0.1980
Fmincon (median)	0.3741	0.4253	0.0000	0.0164	0.0162	0.1679

Table 4.2. Optimal parameter vectors (each row) on “Fantasia” database for different optimization algorithms

4.3.3.3 Performance on test dataset “Fantasia”

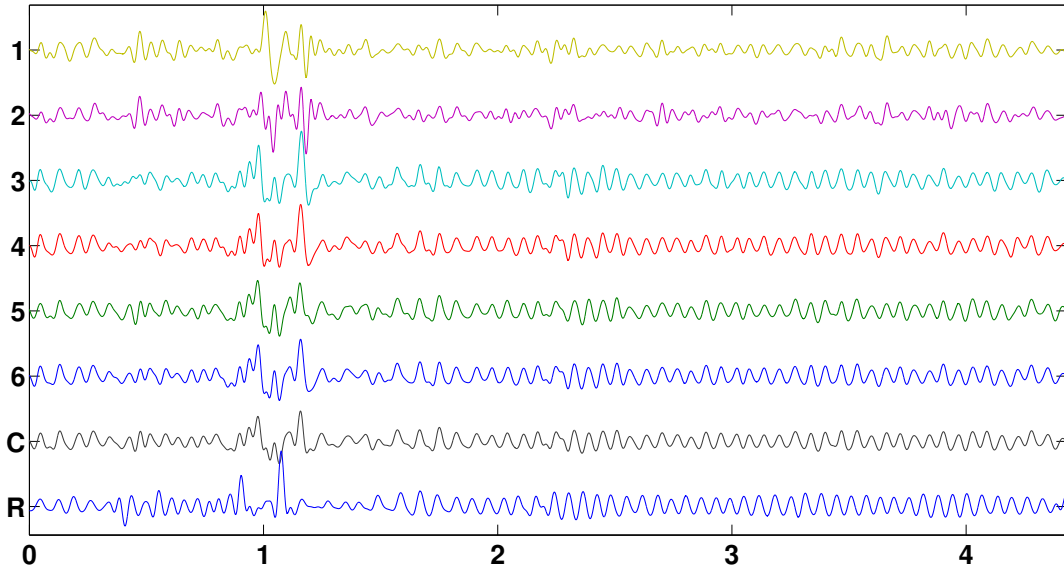


Figure 4.20. Single EDR signals, optimally combined EDR signal and reference signal of an EDR signal from the “Fantasia” database; 1: T peak, 2: T Integral, 3: RS Amplitude, 4: R peak, 5: QRS integral, 6: PCA, C: optimally combined with constant parameter vector, R: reference signal

Since only the Fmincon algorithm uses the information of all signals and also delivers a well performing parameter vector, it is used for the training on the “Fantasia” dataset and validation on the “Slpdb” dataset. In each parameter vector table (see table A.1, table A.2 and table A.3) there are some subjects for which the weighting vector differs significantly from the others (see fig. 4.21 in the appendix) so the median general weighting vector in table 4.2 is used.

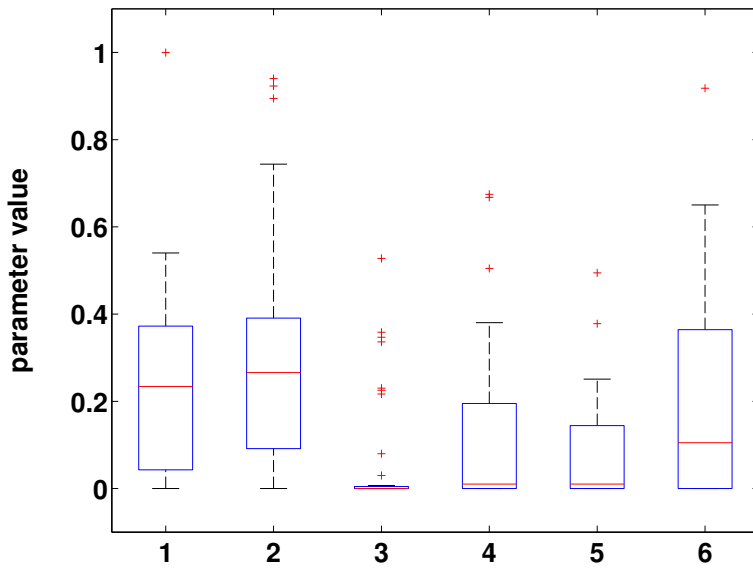


Figure 4.21. Distribution of parameters in the optimal parameter vectors generated by fmincon algorithm for each subject on the Fantasia database (1: PCA, 2: QRS int., 3: R peak, 4: RS ampl., 5: T int., 6: T peak)

The performance of the combined EDR signals compared to the single EDR signals are shown in fig. 4.22. Here the different single methods are listed in the boxplot as boxes 4 to 9 while the best of the single methods for each subject in box 3. Box 1 represent the combined EDR signals with the parameter vector optimized per subject, while box 2 represents the signals with a constant parameter vector for all subjects which was determined in section 4.3.3.2. The combined signal with optimum parameters performs best out of all methods but has the problem that the optimum parameter vector is unknown beforehand so this cannot be used for new signals without a respiratory reference signal. The second best is signal 3 which is only one single method that performs best for each subject. Since it is not possible to know which single EDR method will perform best, this method is also not applicable for new signals. The interesting result is signal 2 with a constant equal weighting vector for all signals. In comparison, this signal performs better than each of the single EDR methods.

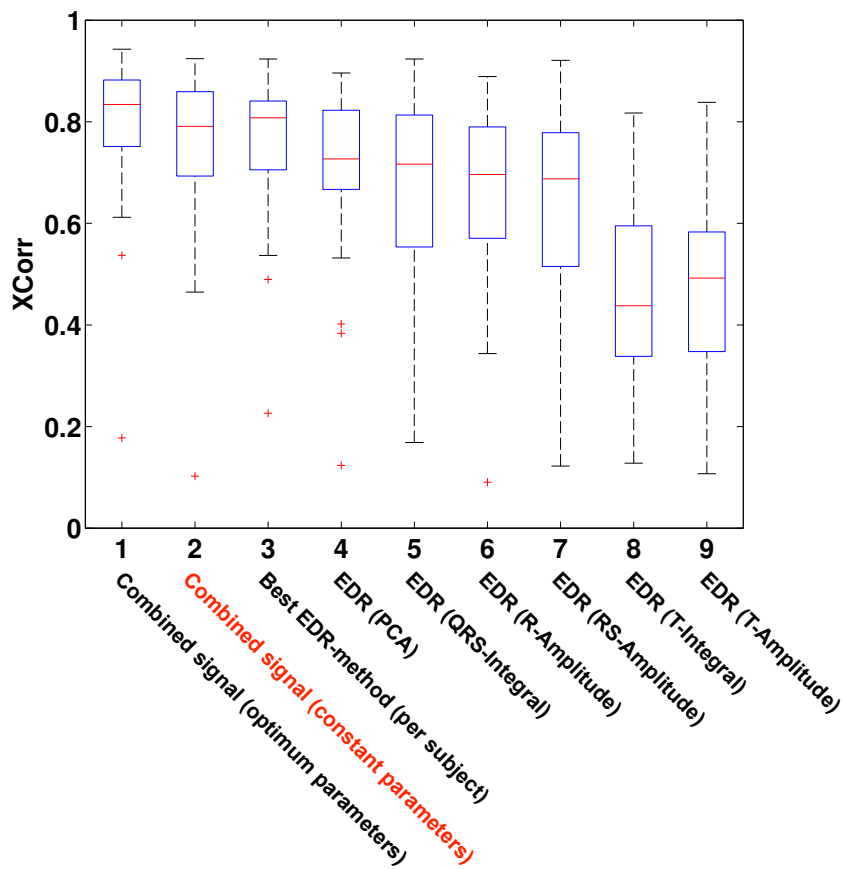


Figure 4.22. Cross-correlation of combined signals and single EDR signals with reference respiratory signal (“Fantasia” database)

This is an interesting outcome but is only valid for this “Fantasia” dataset because the parameters are generated from the same dataset.

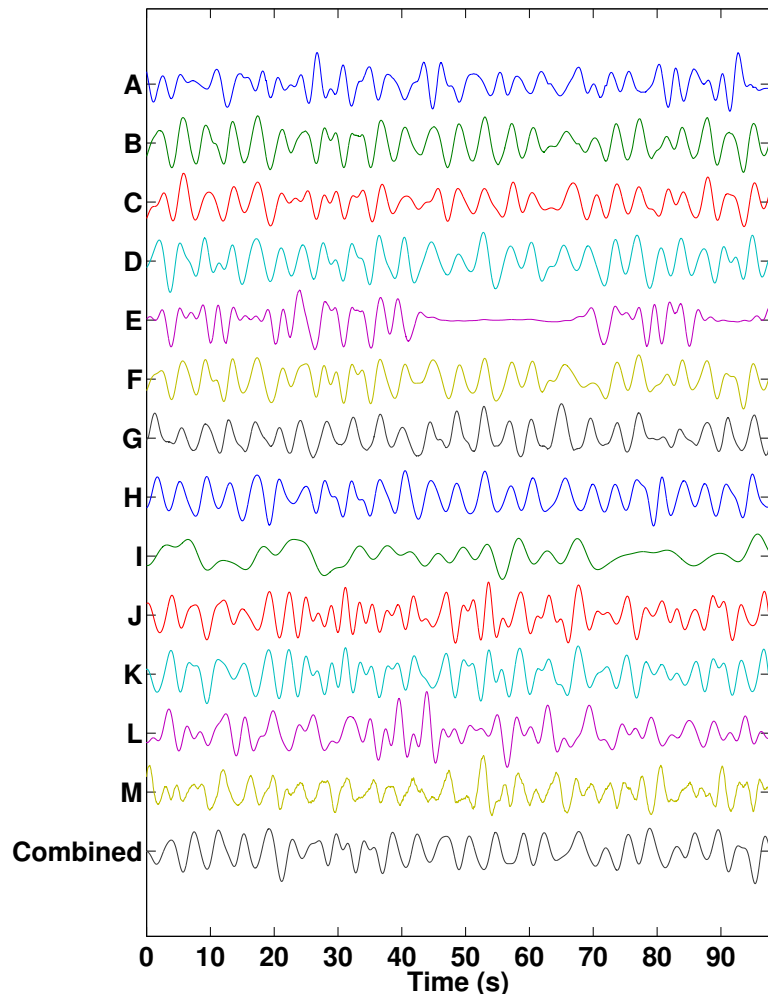


Figure 4.23. Single EDR signals and optimally combined EDR signal of an EDR signal from the “Fantasia” database; A: Kurtosis, B: PCA, C: QRS integral, D: QR slope, E: QRS width, F: R peak, G: RR interval, H: RS amplitude, I: RT peak, J: T integral, K: T peak, L: T slope, M: Wavelet, Combined: optimally combined with constant parameter vector

For verification, the same parameter vector has to be tested on a different dataset. Here the “Slpdb” dataset has been chosen. The results are plotted in fig. 4.24 with the same signals as in fig. 4.22 but generated from this particular dataset. The optimally combined signal performs best and the best single method performs second best just like in the “Fantasia” dataset. Interestingly, signal 2 is likewise performing better than each of the single EDR methods even though the weighting vector generated by the “Fantasia” database is used.

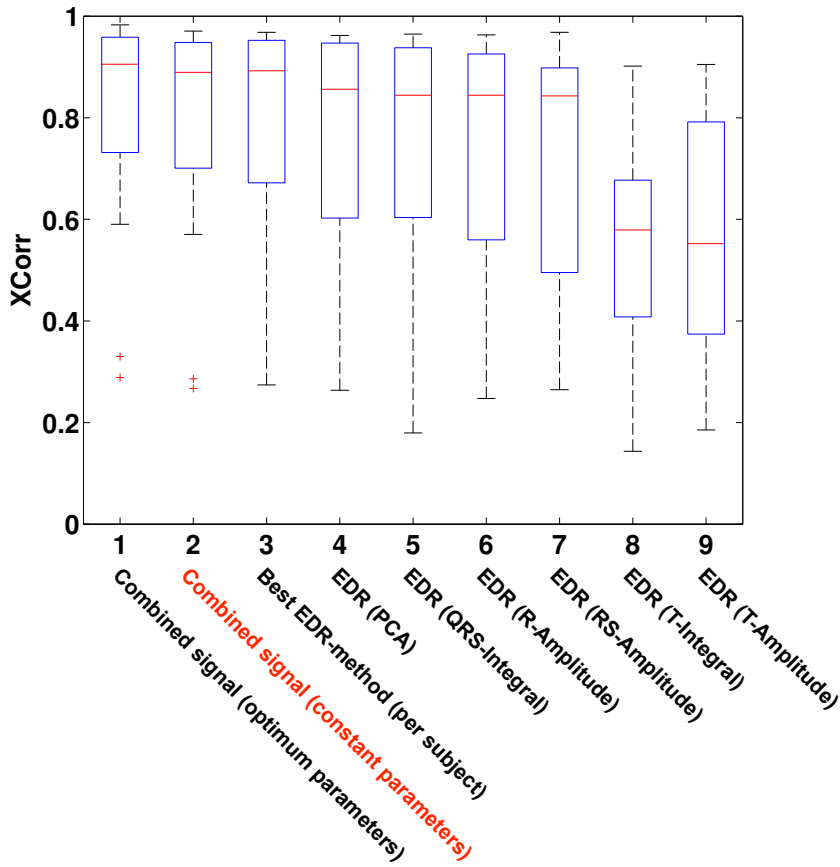


Figure 4.24. Cross-correlation of combined signals and single EDR signals with reference respiratory signal (“Slpdb” database)

This means by combining all EDR methods with a constant parameter vector for all signals, a better EDR signal can be generated than with each of the single methods.

4.4 T wave alternans (TWA)

There exist several methods to detect the T-wave alternans among others STFT-based ones [33] or periodic component analysis (PiCa) [25] methods. The focus of this thesis lies in implementing two methods for further studies. Therefore, the STFT based spectral method has been chosen because of its wide adoption and a more recently developed one based on PiCA. T wave alternans is commonly quantified by the alternans amplitude V_{alt} measured in μV .

4.4.1 Spectral method

The foundation of this method is the fact that an alternating pattern is visible in the spectrogram of a STFT as a peak at the alternating frequency. The implementation of this method mostly follows [33] with slight modifications. First all N T-waves are extracted out of the ECG signal using a fixed size window with L samples and placed into a $(N \times L)$ -sized matrix. The window size has been chosen to be 250 ms and the start of the window is placed at a fixed point 40 ms after the R point. The next step is the alignment of the T-waves since this improves the results significantly [8]. Therefore, the cross-correlation coefficient between the first T-wave and each other one is generated and the waves are aligned such that the cross-correlation coefficient is maximized. For the STFT computation 128 points are used which is the most common value found in literature. The STFT is now computed over each column of the matrix starting with an observation window that contains the T-waves 1 to 128. Using the columns implies that exactly one point of every T-wave is used to generate one STFT eg. all first points then all second points etc. This way one gets L spectra each with 128 points representing every point in time of the T-wave. These spectra are then reduced to one spectrum by averaging the L spectra so there is only one spectrum for every observation window. Next the observation window is shifted by one T-wave to observe the samples of the 2nd to 129th T-wave. After averaging the second spectrum is generated. By shifting the observation window over all N T-waves $N - 127$ spectra are generated (example plot in fig. 4.25). If there is alternans in the T-waves this information is in the spectrogram at exactly 0.5 cycles/beat which corresponds to a period of 2 beats. This is the 65th value of the STFT.

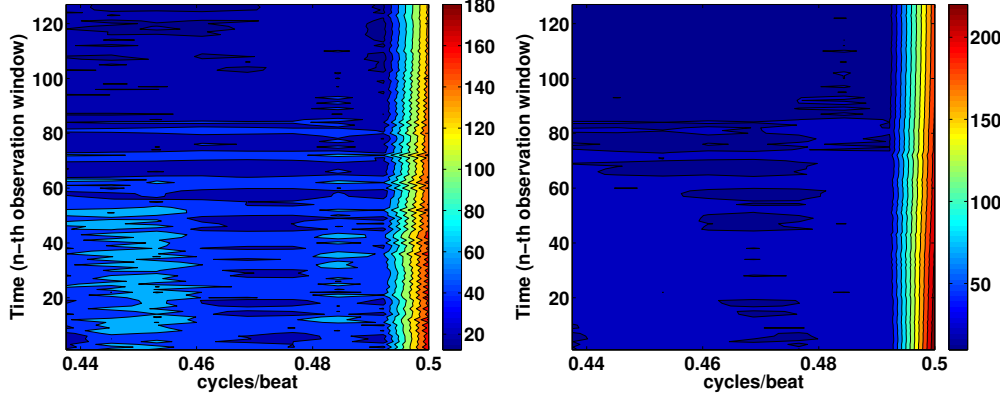


Figure 4.25. Spectrogram of one twadb dataset with different TWA levels in different leads

To estimate the spectral noise power S_{noise} the median of the magnitude in the power spectrum at a predefined noise band (0.44 to up to but not including 0.5 cycles/beat) of all $N - 127$ observation windows is used. The median is used here in contrast to the mean used in [33] to suppress outliers because it is assumed that the majority of frequencies contain noise and only a few outliers contain other artefacts and these outliers would significantly change the noise power when using the mean. The alternans voltage V_{alt} can then be calculated with the magnitude of the power spectrum at the frequency 0.5 $S_{0.5}$ by subtracting the estimated noise level S_{noise} (see equation (4.14)). The largest value of all $N - 127$ spectra is used for $S_{0.5}$ because the TWA might not be present at all times.

$$V_{alt} = \sqrt{(S_{0.5} - S_{noise})} \quad (4.14)$$

To estimate the significance of the value V_{alt} in the presence of noise in the spectrogram a value called K-score is introduced [33] that represents the elevation of the spectrum at 0.5 cycles/beat compared to the noise.

$$K = (S_{0.5} - S_{noise})/\sigma_{noise} \quad (4.15)$$

σ_{noise} is the standard deviation of all frequencies in the noise band of all observation windows. The K score is essential because the noise level can vary between recordings (see fig. 4.26).

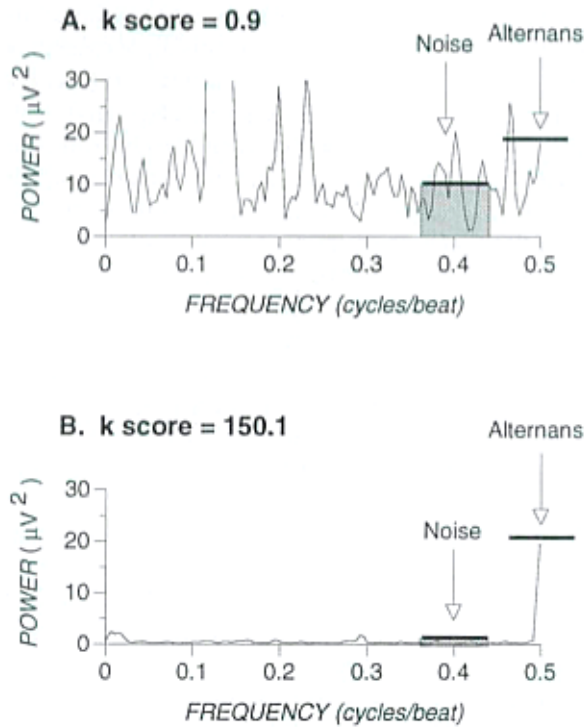


Figure 4.26. Necessity for K score - adapted from [33]

TWA is present and the value regarded significant when a certain empirically defined value of the K-score is exceeded. In [33] this value has been set to 3 so if $K \geq 3$ the TWA value is significant.



Figure 4.27. Block diagram of multilead spectral TWA algorithm

When using this method it is important to always look at all available leads because TWA can be a local phenomenon and thus not necessarily visible to the same extent in all leads (see fig. 4.25). So the algorithm first computes the TWA in all available leads with the K-score and uses the maximum significant TWA (see fig. 4.27).

4.4.2 PiCA method

The method based on periodic component analysis (PiCA) is described in [25]. It is a multilead method that uses all eight linearly independent leads (V1-V6, I, II). We assume a signal with N detected beats and eight leads. First eight signals, one for every lead, with N concatenated T-waves are generated from the original ECG. The start of the T-wave is placed 20 ms after the detected R point and a window after the start is used with the size $t_{window} = 350$ ms. Each signal is then de-trended by subtracting the previous T-wave from the following one so the resulting signal contains $N - 1$ T-waves.

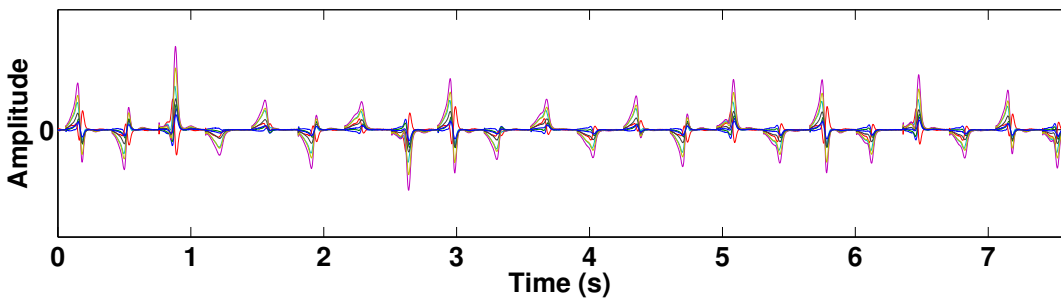


Figure 4.28. Detrended T-wave series of all leads of one signal with alternans visible

All resulting eight detrended signals (see fig. 4.28) are then fed into PiCA with the period T_{PiCA} of

$$T_{PiCA} = 2 \cdot t_{window} \quad (4.16)$$

The output signals are a linear combination of all input signals defined by the eigenvectors that compose the transformation matrix. That way all TWA periodicity is projected to signal described by the first eigenvector (see fig. 4.29). If you compare this signal to the untransformed lead with the most periodicity (see fig. 4.30) you can see the periodicity is much more regular in the transformed lead.

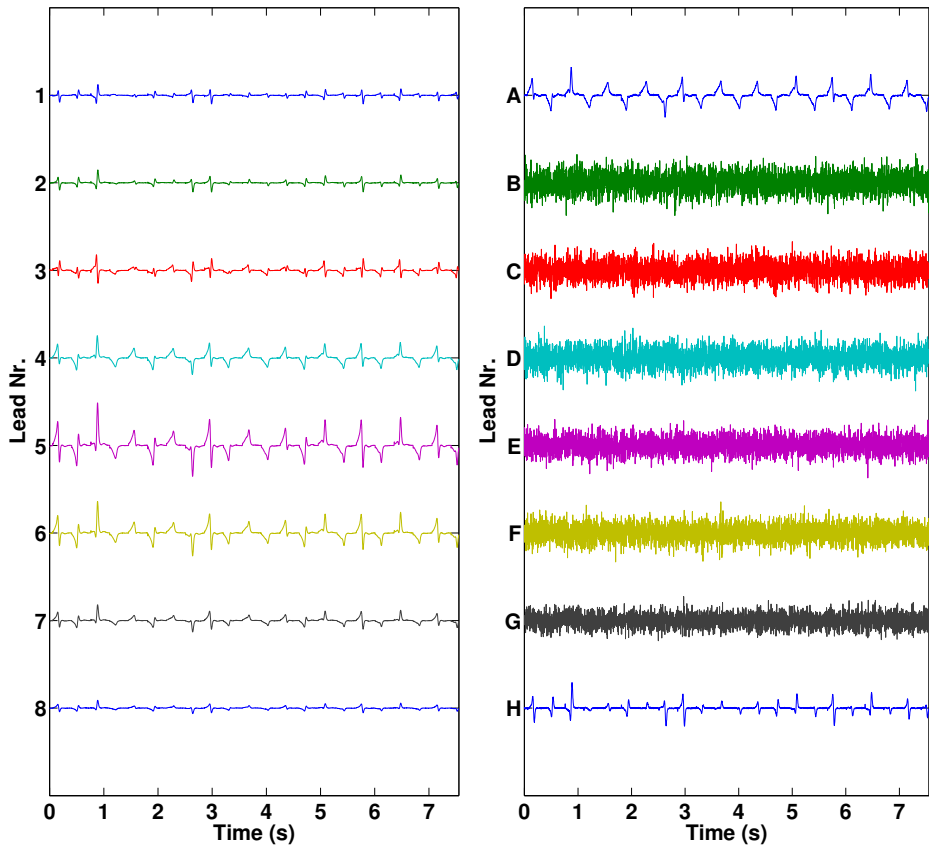


Figure 4.29. Original 8 independent leads (left), PiCA transformed leads (right)

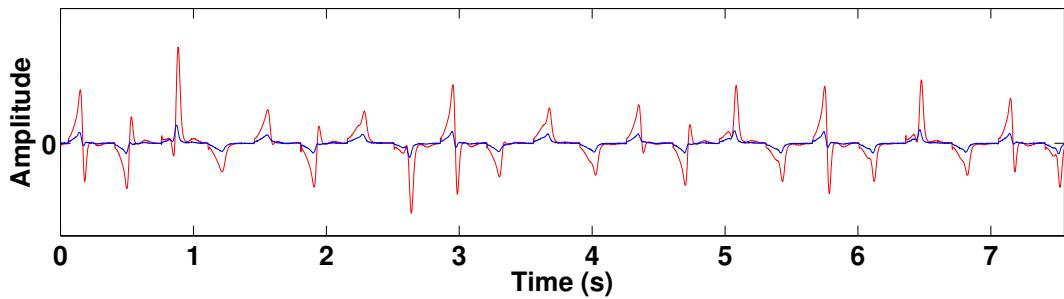


Figure 4.30. Detrended T-wave series of lead with the largest TWA (red) and signal created with first eigenvector (blue)

Since the PiCA transformation to another space does change the amplitude to a different scale the TWA detection has to be done in the original leads [25]. Therefore, the signal is transformed back but only using the first PiCA lead where the alternans is concentrated so only the parts contributing to the

alternans are projected back to the original space. The quantification of alternans is done with the spectral method so the block diagram of the algorithm looks like fig. 4.31. It is an added intermediate step to the spectral method. The major drawback with this method is that the TWA quantification has to be done in the original leads but that is due to the common definition and quantification of TWA in mV so the full potential of this method can not be exploited.

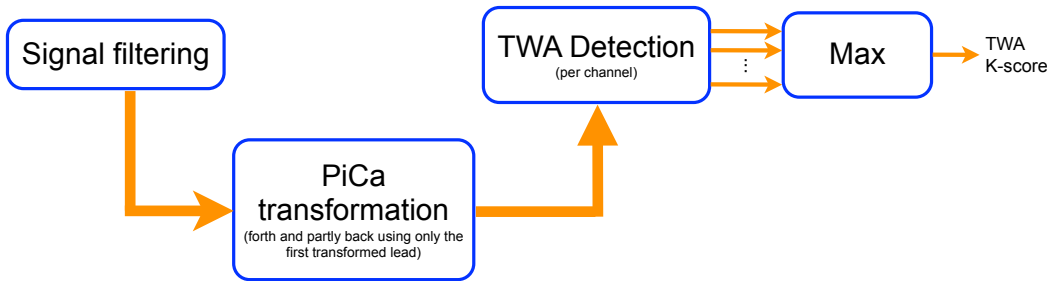


Figure 4.31. Block diagram of multilead PiCA TWA algorithm

4.4.3 Performance

The performance of the two implemented methods has been compared using the “T-Wave Alternans Challenge Database” (see section 4.1.3). For both methods all available independent leads of each subject are used to get a value for the alternans amplitude and the K-score. The dataset is ordered by the amount of detected alternans during the challenge before analysing so the first subject contains the least alternans, the last subject the most. The results of the performance benchmark show no tendency that the higher number datasets have higher absolute TWA values however when looking at the K-score there is a clear tendency visible in both the spectral and the PiCA method (see fig. 4.32). An interpretation for this fact is that in all datasets the alternans level is in the order of the noise level or even below (thus also negative TWA values occur in fig. 4.32 right). The K score can however estimate if the value is significant by including the standard deviation of the noise σ_{noise} . In fact including the K score is the only way to tell if alternans is present.

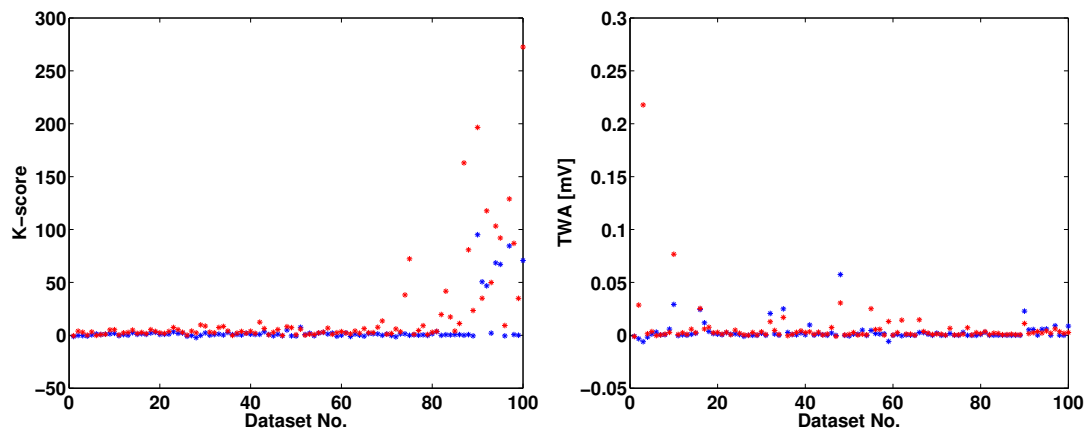


Figure 4.32. K-score (left) and TWA (right) benchmark on “twadb” dataset of spectral method (red) and PiCA method (blue)

Conclusion and prospectives

5.1 EDR

In this thesis different EDR algorithms have been implemented, tested and compared with the goal which is to find a way to improve them by means of exploiting the common information contained in all EDR signals. The first step was to identify already known EDR algorithms and implement them. In that phase, 13 different algorithms were found with different approaches to get a respiratory signal from an ECG. Different benchmark methods were constructed to compare their performances. Based on the benchmark results the best performing EDR algorithms were selected to find a way of getting a better respiratory signal by means of their combination. Therefore, a linear approach was chosen where each signal is weighted by a constant factor and subsequently all signals are put together by summation. The unknown weighting vector was first calculated on a per subject base to show that an improvement with this approach is possible in general. Thereafter, a parameter vector was created which is constant for all subjects. A benchmark with this constant vector also showed an improvement of the resulting respiratory signal when used on the same dataset it was created from. To see if the same constant weighting vector can be used for entirely new subjects while still leading to an improvement, a second database with known respiratory signals was benchmarked. The results showed that even for the new signals this method performed better than each of the single EDR methods. This leads to the conclusion that it is possible to improve an EDR signal by utilizing information of different independent EDR algorithms and merging signals generated by them.

In this thesis 6 out of the 13 algorithms have been chosen for the combination. Possibly even better results can be achieved by combining all of

the 13 algorithms together. The weighting vector is constant for all signals in this thesis. Future projects could focus on finding ways to predict which algorithm works best for certain types of signals by analyzing patterns in the ECG signal. This information can then be used to create an individual weighting vector. Additionally the performance could be increased by using all available leads since in this thesis only one lead is used for each subject.

5.2 T-wave alternans

The purpose of the second part of the thesis was to implement an algorithm to detect and quantify microvolt T-wave alternans for further studies. Since only one algorithm had to be implemented, the oldest and most widely adopted spectral method was chosen. In addition, a more recently developed method (based on the PiCA) which aims on reducing noise in the signal was implemented. In the course of this thesis several problems have been detected with regard to the topic of TWA. TWA in general is still a more recent research area which is not yet completely understood. This implies there are only few studies and more importantly, few datasets available for the development of suitable algorithms. The primary problem is the inconsistent definitions on how the alternans has to be measured. Different algorithms hence lead to different results depending on which alternans characteristics the algorithm is focussed on. Some methods in literature use the maximum difference between two T-waves, others like the spectral method use the average difference over the whole wave. It is easy to understand that a small change which is distributed over the whole wave has little effect, if only the maximum difference is considered. On the other hand if there are T-waves that differ only at a narrow time span but with a large amplitude, they are averaged out by averaging methods. It has to be determined which of these peculiarities exactly are good predictors for sudden cardiac death. At the moment, all changes of the T-wave, be it in amplitude, shape or duration, are projected in only one feature, the amplitude. For the development and verification of new features, more datasets with known cardiac mortality rates of the subjects like seen in [32] are needed. With these datasets new parameters can be developed that characterize the TWA in a better fashion than only by the amplitude. Relative parameters for example the comparison of alternans in the T-wave and in the QRS-complex would make it possible to exploit the full potential of more sophisticated methods like the PiCA and possibly others.

When the research community stays with the current amplitude parameter to quantify TWA, a common definition has to be established. Then all algorithms can be trimmed to look for the same peculiarity and should yield comparable values even when using different algorithms. After a proper definition has been established, algorithms in the time domain like the modified moving average (MMA) method mentioned in [32] can be evaluated.

A larger topic is the detection of irregular alternans patterns and their compensation. Another occurrence to be taken into account are ectopic beats since they can have a significant influence on the detection of TWA [41]. They can cause alternans patterns like A-B-A-B-P-B-A-B-A where P is a premature beat that causes a phase shift of π . If such a beat occurs in the middle of a 128 window in the spectral method the alternans is obscured completely. Algorithms that compensate for such irregularities need to be developed to make the methods more robust.

A

Appendix

PCA	QRS-Int.	R-Peak	RS-Ampl.	T-Int.	T-Peak
0.00122	0.35902	0.35834	0.02211	0.18154	0.07776
0.49083	0.18563	0.00019	0.00001	0.02350	0.29984
0.45078	0.37216	0.00249	0.17448	0.00003	0.00005
0.00000	0.57987	0.00000	0.26618	0.15393	0.00001
0.00009	0.55748	0.21668	0.22568	0.00004	0.00004
0.00175	0.89442	0.00005	0.00005	0.05950	0.04424
0.27368	0.19329	0.33621	0.00077	0.19599	0.00007
0.37277	0.34627	0.00000	0.03646	0.04216	0.20234
0.25611	0.74379	0.00000	0.00009	0.00000	0.00000
0.39293	0.11090	0.00002	0.21575	0.00002	0.28038
0.18631	0.29658	0.00000	0.24177	0.17858	0.09676
0.10012	0.24231	0.00001	0.00994	0.14125	0.50637
0.54025	0.00000	0.00001	0.00006	0.19500	0.26468
0.48162	0.19846	0.00002	0.00007	0.09347	0.22636
0.00003	0.29974	0.07973	0.16205	0.00003	0.45841
0.00001	0.32529	0.00000	0.67468	0.00000	0.00001
0.30751	0.07635	0.00000	0.10883	0.07884	0.42847
0.23419	0.61852	0.00004	0.01054	0.00187	0.13485
0.37212	0.36664	0.00046	0.00001	0.14747	0.11330
0.49840	0.00002	0.00698	0.00000	0.49457	0.00003
0.19055	0.07695	0.00001	0.66760	0.06487	0.00002
0.17324	0.27231	0.34705	0.00001	0.20724	0.00015
0.17348	0.18391	0.23021	0.01087	0.37805	0.02349
0.00012	0.25960	0.52777	0.00007	0.00673	0.20570
0.99973	0.00000	0.00000	0.00001	0.00001	0.00024
0.07687	0.92302	0.00003	0.00001	0.00001	0.00005
0.31848	0.63530	0.00002	0.00001	0.00002	0.04618
0.24744	0.24795	0.00000	0.50459	0.00001	0.00001
0.44207	0.33254	0.22537	0.00000	0.00001	0.00001
0.29621	0.03985	0.00001	0.00002	0.01357	0.65033
0.45512	0.02392	0.00000	0.38024	0.00007	0.14065
0.00001	0.93994	0.00001	0.04068	0.01935	0.00002
0.00022	0.10614	0.02988	0.36798	0.00001	0.49578
0.17560	0.40930	0.00003	0.00001	0.25079	0.16428
0.00893	0.04764	0.00001	0.02546	0.00001	0.91795
0.23379	0.15886	0.00004	0.00001	0.00003	0.60728
0.09651	0.33848	0.00001	0.10351	0.00360	0.45789
0.29552	0.00795	0.00001	0.00000	0.07211	0.62442
0.31931	0.68052	0.00004	0.00002	0.00002	0.00010
0.21042	0.00000	0.00000	0.33684	0.00000	0.45273

Table A.1. Optimal parameter vectors (each row) on "Fantasia" database for each subject using Fmincon algorithm

PCA	QRS-Int.	R-Peak	RS-Ampl.	T-Int.	T-Peak
-0.00958	0.35500	0.36127	0.01966	0.17833	0.07617
0.46316	0.12679	0.05614	-0.05759	0.01845	0.27787
0.44448	0.36902	0.00330	0.17206	-0.00636	-0.00478
-0.09140	0.31149	-0.03180	0.22660	0.09175	-0.24696
-0.07693	0.46102	0.23658	0.20457	-0.01157	-0.00934
0.21571	0.50933	-0.19396	-0.02474	0.03331	0.02294
0.25143	0.16994	0.31464	-0.01674	0.19586	-0.05140
0.35440	0.29943	-0.15203	0.04081	0.02300	0.13034
0.43544	0.07861	-0.41752	-0.02319	-0.01833	-0.02691
0.40388	0.09601	-0.23587	0.10517	-0.01697	0.14210
0.26869	0.22146	-0.11222	0.18365	0.12828	0.08569
0.12570	0.23371	-0.09673	0.02049	0.12006	0.40331
0.46739	-0.11756	-0.15826	0.02068	0.08913	0.14698
0.48456	0.13553	-0.12155	-0.02425	0.06557	0.16853
0.10381	-0.23060	-0.11359	-0.15046	0.01847	-0.38307
0.21947	0.18245	-0.33519	0.22042	-0.00831	-0.03416
0.37668	0.07119	-0.26458	0.05172	0.03419	0.20164
-0.28759	-0.43087	0.19083	-0.00689	0.00124	-0.08258
0.38975	0.29205	-0.03350	-0.08970	0.11545	0.07954
-0.46282	0.05023	0.02082	0.15269	-0.28011	0.03333
0.40840	0.03867	-0.25144	0.19955	0.05646	-0.04547
0.14433	0.17068	0.31054	-0.10566	0.15302	-0.11577
0.17284	0.18462	0.23991	0.00142	0.37787	0.02334
-0.02041	0.22904	0.51691	-0.04445	0.00873	0.18046
0.36424	-0.01500	-0.19943	0.07899	-0.04241	0.29992
-0.17626	-0.53524	0.08027	0.06593	0.06267	-0.07963
0.33792	0.41389	0.01426	-0.13857	-0.02574	0.06962
-0.20470	-0.11030	0.17255	-0.25164	-0.09150	0.16930
0.46044	0.22566	0.15844	-0.13131	-0.02381	-0.00034
0.33654	0.04003	-0.26575	-0.00392	0.00242	0.35135
0.48325	0.01024	-0.17015	0.24013	0.00924	0.08700
-0.19977	0.40059	-0.09657	0.23354	0.05510	0.01444
-0.01674	-0.07448	0.00433	-0.20017	0.14733	-0.55694
0.33200	0.23273	-0.12798	-0.10306	0.12424	0.07999
-0.01801	-0.03232	0.02620	-0.01641	0.02032	-0.88674
-0.18555	-0.06255	-0.04539	0.07695	0.15378	-0.47578
-0.12473	-0.30701	0.11624	-0.07308	0.03076	-0.34819
0.46118	-0.00827	-0.06006	-0.09996	0.06583	0.30470
0.24541	0.15288	-0.38485	-0.04968	0.00524	-0.16195
0.27632	0.03211	-0.23429	0.07859	-0.09226	0.28644

Table A.2. Optimal parameter vectors (each row) on "Fantasia" database for each subject using Least Squares algorithm

PCA	QRS-Int.	R-Peak	RS-Ampl.	T-Int.	T-Peak
0.00000	0.36000	0.36119	0.01949	0.18166	0.07765
0.49315	0.18281	0.00000	0.00000	0.02401	0.30002
0.45034	0.37266	0.00281	0.17419	0.00000	0.00000
0.00000	0.57984	0.00000	0.26612	0.15404	0.00000
0.00000	0.55579	0.21642	0.22778	0.00000	0.00000
0.00103	0.89525	0.00000	0.00000	0.05932	0.04440
0.27452	0.19210	0.33745	0.00000	0.19593	0.00000
0.37536	0.34408	0.00000	0.03618	0.04229	0.20209
0.25725	0.74275	0.00000	0.00000	0.00000	0.00000
0.39365	0.11080	0.00000	0.21546	0.00000	0.28010
0.18581	0.29763	0.00000	0.24063	0.17980	0.09613
0.09800	0.24225	0.00000	0.01172	0.14183	0.50620
0.53954	0.00000	0.00000	0.00000	0.19569	0.26477
0.47982	0.20142	0.00000	0.00000	0.09103	0.22774
NaN	NaN	NaN	NaN	NaN	NaN
0.00000	0.32549	0.00000	0.67451	0.00000	0.00000
0.30774	0.07621	0.00000	0.10974	0.07890	0.42741
NaN	NaN	NaN	NaN	NaN	NaN
0.37491	0.36399	0.00000	0.00000	0.14249	0.11861
NaN	NaN	NaN	NaN	NaN	NaN
0.18421	0.07754	0.00000	0.67221	0.06603	0.00000
0.17318	0.27191	0.34698	0.00000	0.20794	0.00000
0.17284	0.18462	0.23991	0.00142	0.37787	0.02334
0.00000	0.25938	0.52780	0.00000	0.00685	0.20597
1.00000	0.00000	0.00000	0.00000	0.00000	0.00000
NaN	NaN	NaN	NaN	NaN	NaN
0.31796	0.63532	0.00000	0.00000	0.00000	0.04672
NaN	NaN	NaN	NaN	NaN	NaN
0.44223	0.33228	0.22550	0.00000	0.00000	0.00000
0.29644	0.03954	0.00000	0.00000	0.01386	0.65015
0.45722	0.02341	0.00000	0.37890	0.00000	0.14046
0.00000	0.94114	0.00000	0.04002	0.01884	0.00000
NaN	NaN	NaN	NaN	NaN	NaN
0.17768	0.40703	0.00000	0.00000	0.25103	0.16426
NaN	NaN	NaN	NaN	NaN	NaN
NaN	NaN	NaN	NaN	NaN	NaN
NaN	NaN	NaN	NaN	NaN	NaN
0.29140	0.00708	0.00000	0.00000	0.07024	0.63128
0.32617	0.67383	0.00000	0.00000	0.00000	0.00000
0.21003	0.00000	0.00000	0.33779	0.00000	0.45218

Table A.3. Optimal parameter vectors (each row) on "Fantasia" database for each subject using LSQ-Nonneg algorithm

List of Figures

2.1	Circuits of the heart - Adapted from [1]	4
2.2	Thoracic cavities (front) - Adapted from [2]	4
2.3	Position of heart and lungs - Adapted from [3]	5
2.4	Position of heart and lungs - Adapted from [4]	5
2.5	The heart (outside) with arrows indicating the blood flow from the right (green) and left (yellow) half - Adapted from [3]	6
2.6	The heart (inside) with arrows indicating the blood flow from the right (green) and left (yellow) half - Adapted from [3]	6
2.7	Development of the K ⁺ equilibrium potential - Adapted from [7]	8
2.8	Course of an action potential (top), ion permeability (middle), net membrane current (bottom) - Adapted from [5]	10
2.9	Excitation components with their action potentials over time - Adapted from [7]	12
2.10	Excitation path with times in [ms] - Adapted from [7]	13
2.11	Description of waves and segments in a typical ECG trace (Einthoven II) - Adapted from [5]	14
2.12	Development of an ECG trace with depolarized (blue) and repolarized (grey) regions - Adapted from [5]	15
2.13	ECG lead configurations for Einthoven and Goldberger leads - Adapted from [5]	16
2.14	ECG lead configuration for Wilson leads - Adapted from [6] ...	17
2.15	A-E: TWA in the ECG and corresponding action potentials at different heart rates (differences highlighted in red), E: ECG alongside two action potential time series at different locations - Adapted from [11]	18

2.16 X-ray during expiration and inspiration with marked ribs - Adapted from [14]	20
2.17 Block diagram of the signal gathered by an ECG	21
2.18 spatial direction ECG leads represent (leads mostly affected by respiration marked red) - Adapted from [16]	22
2.19 Discretization of signals - Adapted from [20]	24
2.20 Excerpt of a sample chirp signal (top), corresponding spectrogram (bottom)	31
2.21 100 observations of a 2-dimensional random value (black), corresponding principal components (arrows - bold and long: 1st PC; fine and short: 2nd PC) of centered (blue) and non-centered (red) PCA	33
2.22 Upsampling steps (time and frequency) - Adapted from [23] . .	35
2.23 Dyadic time-frequency scale of the DWT with the maximum Frequency in the signal F and the sampling time T . (adapted from [23])	37
2.24 DWT expressed as a multirate filter bank (adapted from [23]) . .	38
4.1 Original ECG signal (blue), 200 ms median filtered (red), 200 ms and 600 ms median filtered (green)	42
4.2 Original signal (red), baseline removed signal (blue) in time- (left) and frequency-domain (right))	43
4.3 Original ECG signal (red), median filtered signal (blue) - no visible ST distortion	43
4.4 R-peak amplitude method	46
4.5 Impulse series (blue), low-pass filtered (and amplified for better visibility) impulse series (red)	46
4.6 QRS Integral method	47
4.7 original ECG signal (blue), interpolated RR interval signal (red) with added offset to visualize correlation with modulation	50
4.8 Projection of the coefficients obtained by a PCA from the QRS complexes onto the first score	51
4.9 Scaling function (red) and wavelet function (blue) of the biorthogonal 5.5 wavelet	52
4.10 Scaling function (red) and wavelet function (blue) of the biorthogonal 5.5 wavelet	53
4.11 reference respiratory signal (blue), wavelet EDR signal (red) . .	53

4.12	original respiratory signal (blue), median filtered (6 s window) original respiratory signal (red)	54
4.13	Sample peaks benchmark for one signal of the fantasia database (median score: 0.93)	55
4.14	Sample respiration rate benchmark for one signal of the fantasia database (median score: 0.97)	56
4.15	Sample xcorr benchmark for one signal of the fantasia database (median score: 0.87)	57
4.16	Number of peaks benchmark of all EDR methods on “Fantasia” dataset	58
4.17	Respiration rate benchmark of all EDR methods on “Fantasia” dataset	59
4.18	Xcorr benchmark of all EDR methods on “Fantasia” dataset . .	59
4.19	Cross-correlation of combined signals and single EDR signals with reference respiratory signal (“Fantasia” database)	64
4.20	Single EDR signals, optimally combined EDR signal and reference signal of an EDR signal from the “Fantasia” database; 1: T peak, 2: T Integral, 3: RS Amplitude, 4: R peak, 5: QRS integral, 6: PCA, C: optimally combined with constant parameter vector, R: reference signal	66
4.21	Distribution of parameters in the optimal parameter vectors generated by fmincon algorithm for each subject on the Fantasia database (1: PCA, 2: QRS int., 3: R peak, 4: RS ampl., 5: T int., 6: T peak)	67
4.22	Cross-correlation of combined signals and single EDR signals with reference respiratory signal (“Fantasia” database)	68
4.23	Single EDR signals and optimally combined EDR signal of an EDR signal from the “Fantasia” database; A: Kurtosis, B: PCA, C: QRS integral, D: QR slope, E: QRS width, F: R peak, G: RR interval, H: RS amplitude, I: RT peak, J: T integral, K: T peak, L: T slope, M: Wavelet, Combined: optimally combined with constant parameter vector	69
4.24	Cross-correlation of combined signals and single EDR signals with reference respiratory signal (“Slpdb” database)	70
4.25	Spectrogram of one twadb dataset with different TWA levels in different leads	72
4.26	Necessity for K score - adapted from [33]	73

4.27	Block diagram of multilead spectral TWA algorithm	73
4.28	Detrended T-wave series of all leads of one signal with alternans visible	74
4.29	Original 8 independent leads (left), PiCA transformed leads (right)	75
4.30	Detrended T-wave series of lead with the largest TWA (red) and signal created with first eigenvector (blue)	75
4.31	Block diagram of multilead PiCA TWA algorithm	76
4.32	K-score (left) and TWA (right) benchmark on “twadb” dataset of spectral method (red) and PiCA method (blue)	77

List of Tables

2.1	Duration of ECG segments	16
2.2	Respiration frequencies [18]	22
4.1	Ordered Xcorr benchmark results on "Fantasia" database	60
4.2	Optimal parameter vectors (each row) on "Fantasia" database for different optimization algorithms	65
A.1	Optimal parameter vectors (each row) on "Fantasia" database for each subject using Fmincon algorithm	84
A.2	Optimal parameter vectors (each row) on "Fantasia" database for each subject using Least Squares algorithm	85
A.3	Optimal parameter vectors (each row) on "Fantasia" database for each subject using LSQ-Nonneg algorithm	86

References

- [1] “<http://leavingbio.net/CIRCULATORYSYSTEM/CIRCULATORYSYSTEM.htm>,” (Accessed 8 May 2014).
- [2] G. S. Thompson, *Understanding anatomy & physiology*. F.A. Davis Company, 2013.
- [3] J. A. Hurst, “Anatomy and physiology in a flash! : an interactive, flash-card approach,” c2011. Includes index. - Description based on print version record.
- [4] “Fundamentals of anatomy and physiology for student nurses,” c2011. Includes bibliographical references and index. - Description based on print version record.
- [5] E. Mutschler, H.-G. Schaible, and P. Vaupel, *Anatomie, Physiologie, Pathophysiologie des Menschen*. Stuttgart: Wiss. Verl.-Ges., 6 ed., 2007.
- [6] J. S. Schwegler and C. Bienstein, *Der Mensch - Anatomie und Physiologie*. Stuttgart: Thieme, 1996.
- [7] E. J. Speckmann, J. . Hescheler, and R. . Köhling, *Physiologie*. Elsevier GmbH, Urban & Fischer Verlag, 2008.
- [8] R. Goya-Estebar, O. Barquero-Pérez, M. Blanco-Velasco, A. Caamaño-Fernández, A. García-Alberola, and J. Rojo-Álvarez, “Nonparametric signal processing validation in T-wave alternans detection and estimation,” *IEEE transactions on bio-medical engineering*, vol. 61, pp. 1328—1338, April 2014.
- [9] E. S. Kaufman, J. A. Mackall, B. Julka, C. Drabek, and D. S. Rosenbaum, “Influence of heart rate and sympathetic stimulation on arrhythmogenic T wave alternans,” *Am J Physiol Heart Circ Physiol*, vol. 279, p. 1248, 2000.
- [10] W. Shimizu and C. Antzelevitch, “Cellular and ionic basis for T-wave alternans under long-QT conditions,” *Circulation*, vol. 99, pp. 1499–1507,

- 1999.
- [11] J. M. Pastore, S. D. Girouard, K. R. Laurita, F. G. Akar, and D. S. Rosenbaum, “Mechanism linking T-wave alternans to the genesis of cardiac fibrillation,” *Circulation*, vol. 99, no. 10, pp. 1385–1394, 1999.
 - [12] G. Thews, E. Mutschler, and P. Vaupel, *Anatomie, Physiologie und Pathophysiologie des Menschen*. Stuttgart: Wissenschaftliche Verlagsgesellschaft mbH, 1991.
 - [13] J. A. Hirsch and B. Bishop, “Respiratory sinus arrhythmia in humans: how breathing pattern modulates heart rate,” *American Journal of Physiology-Heart and Circulatory Physiology*, vol. 241, no. 4, pp. H620–H629, 1981.
 - [14] J. T. Flaherty, S. D. Blumenschein, A. W. Alexander, R. D. Gentzler, T. M. Gallie, J. P. Boineau, and M. S. Spach, “Influence of respiration on recording cardiac potentials: Isopotential surface-mapping and vectorcardiographic studies,” *The American journal of cardiology*, vol. 20, no. 1, pp. 21–28, 1967.
 - [15] M. Huck, J. Haueisen, O. Hoenecke, T. Fritschi, U. Leder, and H. Nowak, “QRS amplitude and shape variability in magnetocardiograms,” *Pacing Clin Electrophysiol*, vol. 23, pp. 234–242, 2000.
 - [16] J. Malmivuo and R. Plonsey, *Bioelectromagnetism*, ch. 12-Lead ECG System, pp. 277–289. New York; Oxford: Oxford University Press, 1995.
 - [17] H. Riekkinen and P. Rautaharju, “Body position, electrode level, and respiration effects on the Frank lead electrocardiogram,” *Circulation*, vol. 53, pp. 40–45, 1976.
 - [18] R. F. Schmidt, G. Thews, and F. Lang, *Physiologie des Menschen*. Berlin; Heidelberg; New York: SpringerMedizinVerlagHeidelberg, 2005.
 - [19] F. Puente León, U. Kiencke, and H. Jäkel, *Signale und Systeme*. München: Oldenbourg Verlag, 2011.
 - [20] I. Rennert and B. Bundschuh, *Signale und Systeme: Einführung in die Systemtheorie*. München: Carl-Hanser-Verlag, 2013.
 - [21] E. Herter and W. Lörcher, *Nachrichtentechnik : Übertragung, Vermittlung, Verarbeitung*. München: Hanser, 9., bearb. aufl. ed., 2004. Pb. : EUR 29.90, EUR AT 30.80, CHF 46.70.
 - [22] K. D. Kammerer and K. Kroschel, *Digitale Signalverarbeitung: Filterung und Spektralanalyse*. Studium, Wiesbaden: Vieweg + Teubner, 2009.
 - [23] U. Kiencke, M. Schwarz, and T. Weickert, *Signalverarbeitung: Zeit-Frequenz-Analyse und Schätzverfahren*. München: Oldenbourg, 2008.

- [24] R. Sameni, C. Jutten, and M. B. Shamsollahi, "Multichannel electrocardiogram decomposition using periodic component analysis," *IEEE Transactions on bio-Medical Engineering*, vol. 55, pp. 1935–1940, 2008.
- [25] V. Monasterio, G. D. Clifford, P. Laguna, and J. P. Martinez, "A multilead scheme based on periodic component analysis for T-wave alternans analysis in the ECG," *Annals of Biomedical Engineering*, vol. 38, pp. 2532–2541, 2010.
- [26] R. C. Gonzalez and R. E. Woods, *Digital image processing*. World students series, Reading Menlo Park New York: Addison-Wesley, 1993.
- [27] P. De Chazal, C. Heneghan, E. Sheridan, R. Reilly, P. Nolan, and M. O'Malley, "Automated processing of the single-lead electrocardiogram for the detection of obstructive sleep apnoea," *Biomedical Engineering, IEEE Transactions on*, vol. 50, no. 6, pp. 686–696, 2003.
- [28] S. Dingab, X. Zhua, W. Chena, and D. Weia, "Derivation of respiratory signal from single-channel ECGs based on Source Statistics," 2004.
- [29] P. Langley, E. J. Bowers, and A. Murray, "Principal Component Analysis as a Tool for Analyzing Beat-to-Beat Changes in ECG Features: Application to ECG-Derived Respiration," *IEEE Transactions on Biomedical Engineering*, vol. 57, pp. 821–829, 2010.
- [30] C. Avci, S. Besli, and A. Akbas, "Performance of the EDR methods: evaluations using the mean and instantaneous respiration rates," in *Bioinformatics and Biomedical Engineering, (iCBBE) 2011 5th International Conference on*, pp. 1–5, IEEE, 2011.
- [31] A. E. Santo and C. Carbajal, "Respiration rate extraction from ECG signal via discrete wavelet transform," in *Circuits and Systems for Medical and Environmental Applications Workshop (CASME), 2010 2nd*, pp. 1–4, IEEE, 2010.
- [32] T. Nieminen and R. L. Verrier, "Usefulness of T-Wave Alternans in Sudden Death Risk Stratification and Guiding Medical Therapy," *Annals of Noninvasive Electrocardiology*, vol. 15, no. 3, pp. 276–288, 2010.
- [33] D. S. Rosenbaum, P. Albrecht, and R. J. Cohen, "Predicting Sudden Cardiac Death From T Wave Alternans of the Surface Electrocardiogram," *Journal of cardiovascular electrophysiology*, vol. 7, no. 11, pp. 1095–1111, 1996.
- [34] L. K. Saul and J. B. Allen, "Periodic component analysis: an eigenvalue method for representing periodic structure in speech," in *Nips*, pp. 807–813, 2000.

- [35] A. L. Goldberger, L. A. Amaral, L. Glass, J. M. Hausdorff, P. C. Ivanov, R. G. Mark, J. E. Mietus, G. B. Moody, C. K. Peng, and H. E. Stanley, “PhysioBank, PhysioToolkit, and PhysioNet: components of a new research resource for complex physiologic signals,” *Circulation*, vol. 101, pp. E215–20, 2000.
- [36] Y. Ichimaru and G. Moody, “Development of the polysomnographic database on CD-ROM,” *Psychiatry and Clinical Neurosciences*, vol. 53, no. 2, pp. 175–177, 1999.
- [37] N. Iyengar, C. Peng, R. Morin, A. L. Goldberger, and L. A. Lipsitz, “Age-related alterations in the fractal scaling of cardiac interbeat interval dynamics,” *American Journal of Physiology-Regulatory Integrative and Comparative Physiology*, vol. 40, no. 4, p. R1078, 1996.
- [38] G. Moody, “The physionet/computers in cardiology challenge 2008: T-wave alternans,” in *Computers in Cardiology, 2008*, pp. 505–508, IEEE, 2008.
- [39] G. Lenis, “Automatic detection and classification of ectopic beats in the ECG using a Support-Vector-Machine,” Studienarbeit, Institut für Biomedizinische Technik, Karlsruher Institut für Technologie (KIT), Kartlsruhe, 2010.
- [40] F. Puente León, *Messtechnik: Systemtheorie für Ingenieure und Informatiker*. Berlin, Heidelberg: Springer, 2011.
- [41] D. M. Bloomfield, S. H. Hohnloser, and R. J. Cohen, “Interpretation and classification of microvolt T wave alternans tests,” *Journal of cardiovascular electrophysiology*, vol. 13, no. 5, pp. 502–512, 2002.